A comprehensive pharmacological survey across heterogeneous patient-derived GBM stem cell models.

Richard J.R. Elliott[1], Peter W.K. Nagle[1], Muhammad Furqan[1], John C. Dawson[1], Vanessa Smer-Barreto[1,2], Diego A. Oyarzún[2,3], Aoife McCarthy[1], Alison F. Munro[1], Camilla Drake[1], Gillian M. Morrison[4], Steven M. Pollard[4], Michael Marand[1], Daniel Ebner[5], Val Brunton[1], Margaret C. Frame[1] and Neil O. Carragher[1]

[1] Cancer Research UK Scotland Centre (Edinburgh), Institute of Genetics and Cancer, University of Edinburgh, Western General Hospital, Edinburgh, UK.

[2]School of Informatics, University of Edinburgh, 10 Crichton St, Edinburgh, EH8 9AB, UK.

[3]School of Biological Sciences, University of Edinburgh, Max Born Crescent, Edinburgh, EH9 3BF, UK.

[4]Institute of Regeneration and Repair, Cancer Research UK Scotland Centre, University of Edinburgh, EH16 4UU, U.K.

[5]Nuffield Dept. Of Medicine, University of Oxford, Old Road Campus, Oxford OX3 7BN, U.K.

Address for correspondence:

Prof Neil Carragher:

Edinburgh Cancer Research,

Institute of Genetics and Cancer,

University of Edinburgh,

Western General Hospital,

Edinburgh, UK. EH4 2XR

Tel: +44 (0)131 6518671

Email: n.carragher@ed.ac.uk

Abstract

Despite substantial drug discovery investments, the lack of any significant therapeutic advancement in the treatment of glioblastoma (GBM) over the past two decades calls for more innovation in the identification of effective treatments. The inter- and intra-patient heterogeneity of GBM presents significant obstacles to effective clinical progression of novel treatments by contributing to tumour plasticity and rapid drug resistance that confounds contemporary target directed drug discovery strategies. Phenotypic drug screening is ideally suited to heterogeneous diseases, where targeting specific oncogenic drivers have been broadly ineffective. Our hypothesis is that a modern phenotypic led approach using disease relevant patient-derived GBM stem cell systems will be the most productive approach to identifying new therapeutic targets, drug classes and future drug combinations that target the heterogeneity of GBM. In this study we incorporate a panel of patient-derived GBM stem cell lines into an automated and unbiased 'Cell Painting' assay to quantify multiple GBM stem cell phenotypes. By screening several compound libraries at multiple concentrations across a panel of patient-derived GBM stem cells we provide the first comprehensive survey of distinct pharmacological classes and known druggable targets, including all clinically approved drug classes and oncology drug candidates upon multiple GBM stem cell phenotypes linked to cell proliferation, survival and differentiation. Our data set representing, 3866 compounds, 2.2million images and 64000 datapoints is the largest phenotypic screen carried out to date on a panel of patient-derived GBM stem cell models that we are aware of. We seek to identify agents and target classes which engender potent activity across heterogenous GBM genotypes and phenotypes, in this study we further characterize two validated target classes, histone deacetylase inhibitors and cyclin dependent kinases that exert broad and potent effects on the phenotypic and transcriptomic profiles of GBM stem cells. Here we present all validated hit compounds and their target assignments for the GBM community to explore.

Introduction

Glioblastoma (GBM), a Grade IV astrocytoma, is a highly complex disease that remains difficult to treat. Mortality rates have increased over the last 30 years, especially in the over 60 age group, as incidence rates outpace survival improvements [1]. GBM is therefore the most common and aggressive primary malignant tumour of the brain and represents an urgent area of unmet medical need. Since the introduction of post-surgical, concomitant radiotherapy and adjuvant temozolomide in 2005 (the 'Stupp protocol'), which increased median overall survival (mOS) by ~3 months[2], a lack of effective, novel treatments for GBM have been introduced into broad clinical use and 5-year survival rates from time of diagnosis remain at less than 5%[3]. Clinical and scientific research over the last 20 years has revealed a complex landscape of remarkable intra- and inter-tumoral heterogeneity associated with the highly dynamic nature of GBM molecular biology [4, 5{Verhaak, 2010 #312{Brennan, 2013 #313, 6, 7]. The complex biology driving the disease is further exacerbated by the addition of GBM stem cells (GSC), driving self-renewal and resistance mechanisms[8-13]. The self-renewing capacity of GSCs is an inherent feature of GBM to which the tumour microenvironment, or the GBM stem cell niche, contributes by supporting adaptive signal rewiring, heterogeneous tumour evolution and therapeutic resistance[14, 15]. Phospho-proteomic studies performed on patient derived GBM model systems demonstrate rapid rewiring of pathway signalling at the post-translational pathway level following effective inhibition of some of the most compelling drug targets such as the mTOR pathway, that is hyperactivated in approximately 90% of GBM[16]. GBM plasticity and heterogeneity thus confound modern target-based drug discovery strategies contributing to drug resistance and relapse, hence the targeting of clear oncogenic drivers of GBM, such as EGFR amplification/mutation or RAS, PI3K signalling, has not translated into significant efficacy in GBM clinical management. Emerging single-cell transcriptomic[17], proteomic[18] and image-based phenotypic screening[19] technologies combined with improved patient-derived GSC models[20] provide new opportunities to understand and overcome disease heterogeneity. New hope for the development of novel therapeutic classes and drug combinations that may overcome some if this heterogeneity and support new personalized treatments strategies for GBM is provided from the recent phase 2 ROAR basket clinical trial study evaluating a combination of a BRAF targeting agent (dabrafenib) and the MEK inhibitor (trametinib) which includes a cohort of 45 high grade glioma (HGG, including GBM) patients with BRAF V600E mutation. The primary endpoint of investigator-assessed overall response rate was 33% in the HGG cohort. Secondary endpoints of median duration of response (DoR), progression-free survival (PFS) and mOS in the HGG cohort was; 31.2, 5.5 and 17.6 months respectively[21]. Emerging case reports from both adult and pediatric patients also point to the benefit of treating BRAF mutation-positive glioblastoma and gliomas with the dabrafenib and trametinib combination[22-25]. However, BRAF V600E mutation can be found in approximately only 3% of GBM patients therefore, while such personalized treatments offer hope, the challenge is addressing the majority of patients which do not fall into molecular subtypes defined by a well-established druggable target or pathway, or are refractory to such personalized treatments.

The drug development of imidazotetrazines, such as temozolomide, extended from chemocentric and phenotypic-led collaborative research exploring the *in vitro* and *in vivo* anti-cancer properties of small molecules, dacarbazine and mitozolomide (azolastone)[26] emphasizing the value of incorporating complex tumour biology into early stage drug design and selection. Phenotypic drug discovery (PDD), defined as the identification of hit or lead compounds prior to target identification[27], has historically contributed more than target-based drug discovery (TDD), in terms of first-in-class drugs approved by the FDA since 1999[28, 29], yet TDD has dominated drug discovery approaches in oncology over the same period of time[30]. While TDD and PDD are complimentary drug discovery strategies, PDD can offer some advantages over target-based methods, as it allows discovery of potential therapeutics using complex, biological models of poorly understood heterogeneous disease states[31, 32] and can reveal novel unprecedented therapeutic

classes such as the first HDAC inhibitor (vorinostat), molecular glues (lenalidomide), spicing modulators (risdiplam)[28, 33] and novel conformation-selective binding modes-of-action for existing targets (NXP900/eCF506)[34]. This 'target-agnostic' approach has been greatly assisted by hardware advances in high-content microscopy, the development of advanced image analysis software tools and improved phenotypic profiling techniques, such as Cell Painting and Artificial Intelligence/Machine Learning (AI/ML) methods that help classify cell phenotypes and elucidate drug mechanism-of-action[35-38]. Recent advances in multiparametric high-content imaging enables the generation of a phenotypic fingerprint for every chemical (or genetic) perturbation to support the new discipline of 'phenotypic (or morphometric) profiling' that quantifies functional similarities and dissimilarities between drug mechanism-of-action (MOA) within intact cell-based assay systems[35, 39-41]. The Cell Painting assay multiplexes six fluorescent dyes, imaged in five spectral channels to reveal eight broadly relevant cellular components or organelles and can be combined with the development of bespoke automated image analysis pipelines to segment individual cells and calculate thousands of morphological feature-based measurements per cell (e.g. various measures of size, shape, texture, intensity and many others) to produce a data-rich profile that is suitable for the detection of subtle cellular phenotypes which can be linked to biological outcomes[42]. Here we describe the adaptation and optimization of Cell Painting for profiling compound MOA and target-class across a panel of 6 genetically distinct GSC lines obtained from the Glioma Cellular Genetics Resource (https://github.com/GCGR). Using this approach we provide a comprehensive pharmacological audit of how specific target, pharmacological and chemical classes influence patient-derived GBM cellular phenotypes. We present a large-scale application of this technique using chemically diverse libraries containing FDA approved drugs, or Phase I passed clinical candidates and selective chemical probe compounds against known oncology targets. We identify multiple diverse pharmacological and target classes effective across our genetically distinct panel of patient-derived GSCs and present all validated screening hits and their target assignments to the GBM research community. These results support our hypothesis that an unbiased phenotypic led approach, using disease relevant patient-derived GSC models and exploitation of deep phenotyping and drug mechanism-of-action profiling technologies is a productive approach to identifying new targets, drug classes and future drug combinations that address the heterogeneity of GBM.

Results

Glioblastoma Stem Cell Models

Patient-derived GSCs were obtained from the Cancer Research UK Glioma Cellular Genetics Resource, and 6 GSC lines were initially selected to cover common transcriptomic subtypes based on their RNA-Seq subtype classification (classical (CLA), mesenchymal (MES), proneural (PRO), Supplementary Figure 1A). GSC's were cultured on laminin-1 coated substrates, under defined media conditions that have previously been demonstrated to maintain their stem cell-like properties[43]. Initial studies demonstrate compatibility with high-content imaging (i.e., flat and adherent morphology) and cell number was optimised for 384-well microtiter plate formats to enable high-throughput drug screening (Supplementary Figure 1B-D). Given the generally slow growth rates of the GSCs relative to standard cancer cell line cultures, compound exposure over 72 hours during screening was selected to ensure at least one population doubling in all lines. Short-tandem repeat (STR) profiling was carried out on each GSC line to create reference sequences and all cell lines were expanded and cell stocks banked in liquid nitrogen, to facilitate screening with consistent low passage numbers ensuring minimal biological drift across primary screening and secondary hit validation assays. In order to begin characterising these cell lines, prior to phenotypic screening we examined basal protein expression and post-translational pathway activation status by Reverse Phase Protein Array (RPPA) and cytokine array in 2-dimensional (2D) and 3-dimensional (3D) cell culture conditions. Basal levels of protein and phospho-epitope abundance (in 2D and 3D culture) show functional enrichment of signalling pathways in MAPK, ErbB, VEGF, PI3K-AKT, focal adhesion, EGFR inhibitor resistance and PD-1 checkpoint in cancer (Supplementary Figure 2). The cytokine

array profiling further demonstrates enrichment in the secretion of GBM associated chemokine proteins involved in tumour progression, invasion, angiogenesis (IL-6, MMP-7, TIMP1, VEGF), and tumour associated neutrophils (TANs; CCL2, IL-8/CXCL8)[44] including factors previously shown to contribute to GSC subtype trans-differentiation (PRO to MES transition)[45]. (Supplementary Figure 2A-D). Notably the six GSC lines representing three pairs of the common GBM transcriptomic sub-types (CLA, MES and PRO) selected for our study do not cluster into any specific subgroups based on basal protein expression or pathway activation status. Interestingly, high levels of the pro-inflammatory cytokine, interleukin-8 (CXCL8, Supplementary Figure 2C, D) has recently been reported as a druggable target in GBM (*via* humanised anti-IL8 antibody) with an anti-PD-1 combinational blockade[46]. Overall, this pre-screening profiling indicates our proposed GSC drug screening models are representative of typical GBM signalling networks observed in patient samples, express known druggable pathways while capturing the expected broad heterogeneity of GBM tumours at the molecular, protein and morphological levels in both 2D adherent and 3D cell culture.

GSC Cell Painting Assay Development

Previously, we have successfully adapted the Cell Painting protocol[35, 47] to explore drug MOA across cancer cell line panels from diverse lineages including, breast and oesophageal adenocarcinoma[19, 48, 49]. In the current study, we adapt the protocol to our panel of patient-derived GSCs and incorporate live mitochondrial staining prior to fixation and staining with the remaining Cell Painting reagents (Figure 1A, B). It is our understanding that this study describes the first application of phenotypic profiling using the Cell Painting assay to a panel of patient-derived GSC models. Images from each cell line were then used to build a customized CellProfiler[50] image analysis pipeline and confirm appropriate image segmentation and performance of high content analysis. CellProfiler analysis quantified up to 1006 cellular features from each GSC and principal component analysis was carried out on median aggregated well level data using the StratoMineR HCA platform (stratominer.com). Nuclei Count features were also extracted to assess reproducibility of cell seeding in 384-well format and calculate the percentage cell survival following each compound treatment including signal-to-noise assessment between negative control (0.1% (v/v) dimethylsulfoxide, DMSO) and cytotoxic positive control compounds (paclitaxel, staurosporine). These assay validation studies confirm assay reproducibility and signal-to-noise in 384-well plate formats is suitable for high-throughput screening based on industry-standard recommendations[51] (Supplementary Figures 1C & Supplementary Figure 3).

Our phenotypic screening campaign performed across the panel of six GSC lines incorporated multiple small molecule compound libraries screened against varied concentrations (ranging from 3-10,000nM) (see Table 2 methods section for specific concentrations for each library). Compound libraries included the LOPAC (1280 compounds, Merck), Prestwick FDA (1280 compounds), TargetMol L2110 (330 compounds), Structural Genomics Consortium Kinase Chemogenomic set (KCGS – 295 compounds)[52]) and a custom chemogenomic library set (789 compounds, 'Comprehensive anti-Cancer small Compound Library, or C3L) (Table 1, Materials & Methods). The C3L library was created with a focus on chemical and known oncology target diversity to functionally evaluate known oncology targets across phenotypic screening assays[53]. The majority of these commercially available compounds (across all library sets) have been through phase I clinical trials. It is our view that this approach presents the potential for discovering novel drug repurposing and drug combination opportunities in addition to identifying new therapeutic targets not previously explored in GBM.

192

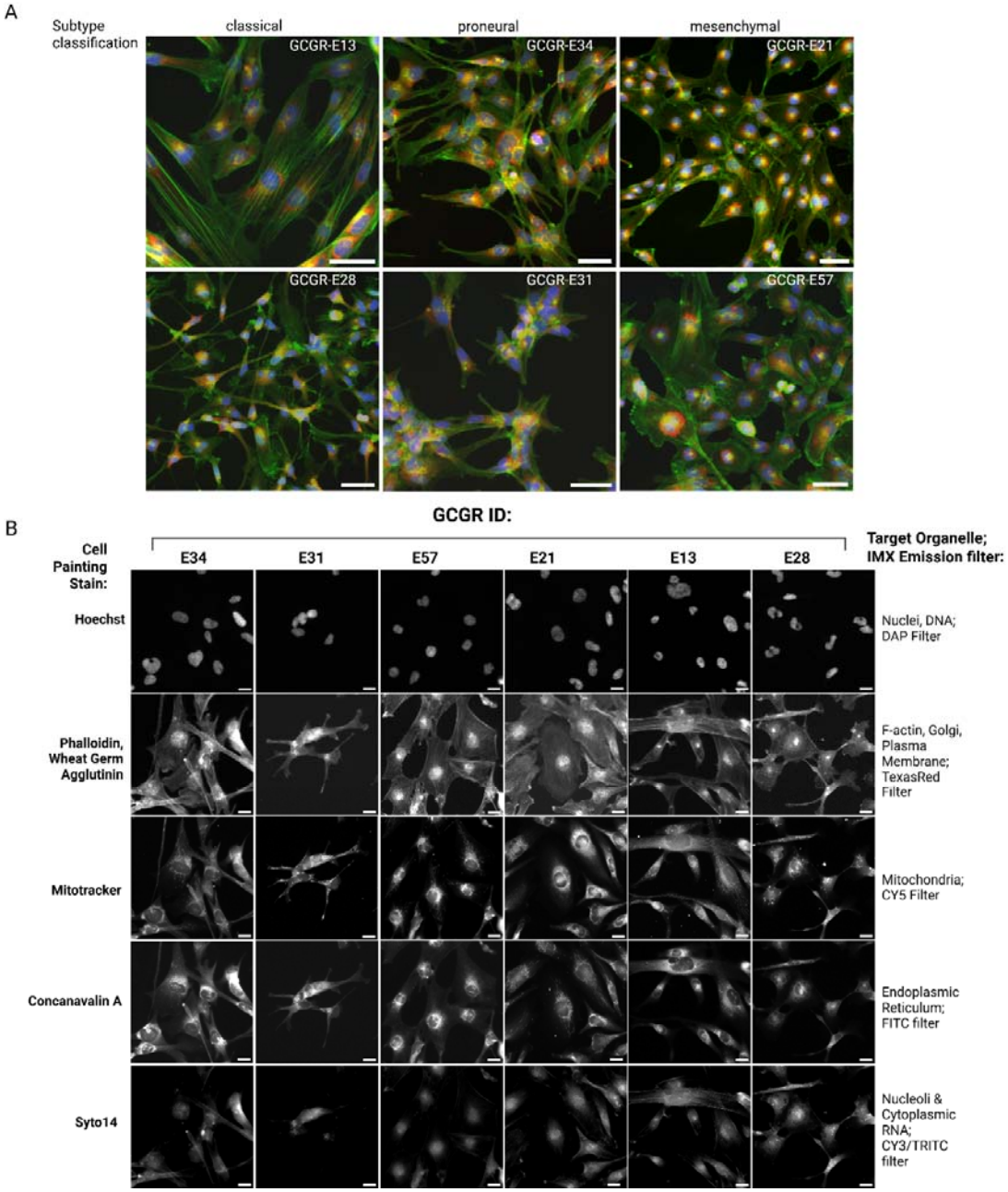

193

194 Figure 1. High content phenotypic assay screening on GSC panel. A. Representative images of Cell Painting across
195 GSC panel (Hoechst (blue), Phalloidin/WGA (green), Endoplasmic reticulum (red). Scale bar 50µM. B.
196 Representative images of individual cell painting stains, target organelle and corresponding filter across GSC panel.
197 Scale bar 20µM.

198

199 *High Content Cell Painting Screen, Analysis & Validation*

200 Our optimised GSC high content phenotypic screening and analysis workflow is outlined (Figure 1C)
201 and described in detail in the material and methods section.

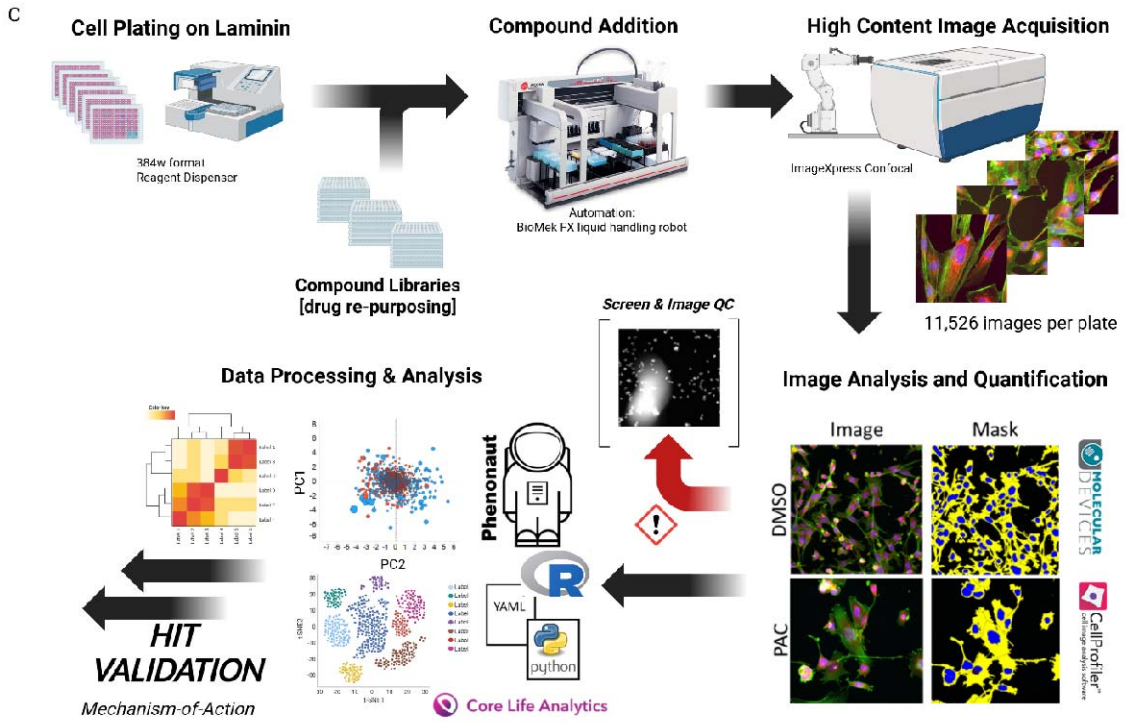

Figure 1 *continued*. C. Established high content screening, image and analysis workflow, followed by subsequent hit validation and exploration.

Briefly, cell lines were seeded (500-1500 cells per well) onto laminin pre-coated 384-well plates, followed by compound addition at 24 hours using automated liquid handling platforms. DMSO was used as a negative (compound vehicle) control (n = 48 wells per plate minimum) with staurosporine (1µM, n= 16) typically used as an assay landmark control for cell death. After 72 hours compound exposure, cells were subjected to live cell labelling of mitochondria with MitoTracker™, followed by fixation, permeabilization, and additional staining with the remaining Cell Painting dyes (see Materials & Methods). Images for phenotypic analysis were acquired using an ImageXpress Confocal high-content microscope with six fields of view (20× objective) over five channels, collecting 11,520 images per 384-well plate. Each compound library was screened separately across all six GCGR cells lines. In total 3,866 compounds were screened (varied doses), ~2.2 million images collected (21 Tb) representing a dataset of >62,000 datapoints. Image analysis was carried out *via* a custom CellProfiler pipeline and secondary multiparametric data analysis was performed using StratoMineR™ (Core Life Analytics)[54] and TIBCO Spotfire® software (Revvity) - see methods. Representative principal component plots (PC1-3 of 20 principal components, covering >60% of explained variance) were created for LOPAC, Prestwick and C3L libraries (Figure 2, panels A, B, C & Supplementary Figure 4) to visualize distribution of active compounds from DMSO controls in phenotypic space. Further dimensionality reduction of these principal components was carried out, creating a phenotypic (Euclidean) distance for each compound, dose and cell line, relative to DMSO controls. The corresponding *p*-value to this phenotypic distance was plotted against cell survival (z-scores), based on DMSO normalised nuclei counts (Figure 2D, E & F). Standard high-throughput screening (HTS) quality control assessments were also carried out *via* Nuclei Count outputs from DMSO and staurosporine controls i.e., signal-to-noise *via* Z-prime robust (>0.35 minimum) across each plate (Supplementary Table 2). Image quality modules in CellProfiler were used to flag artefacts/blurred images, as well as additional compound triage *via* direct image assessment for putative hits.

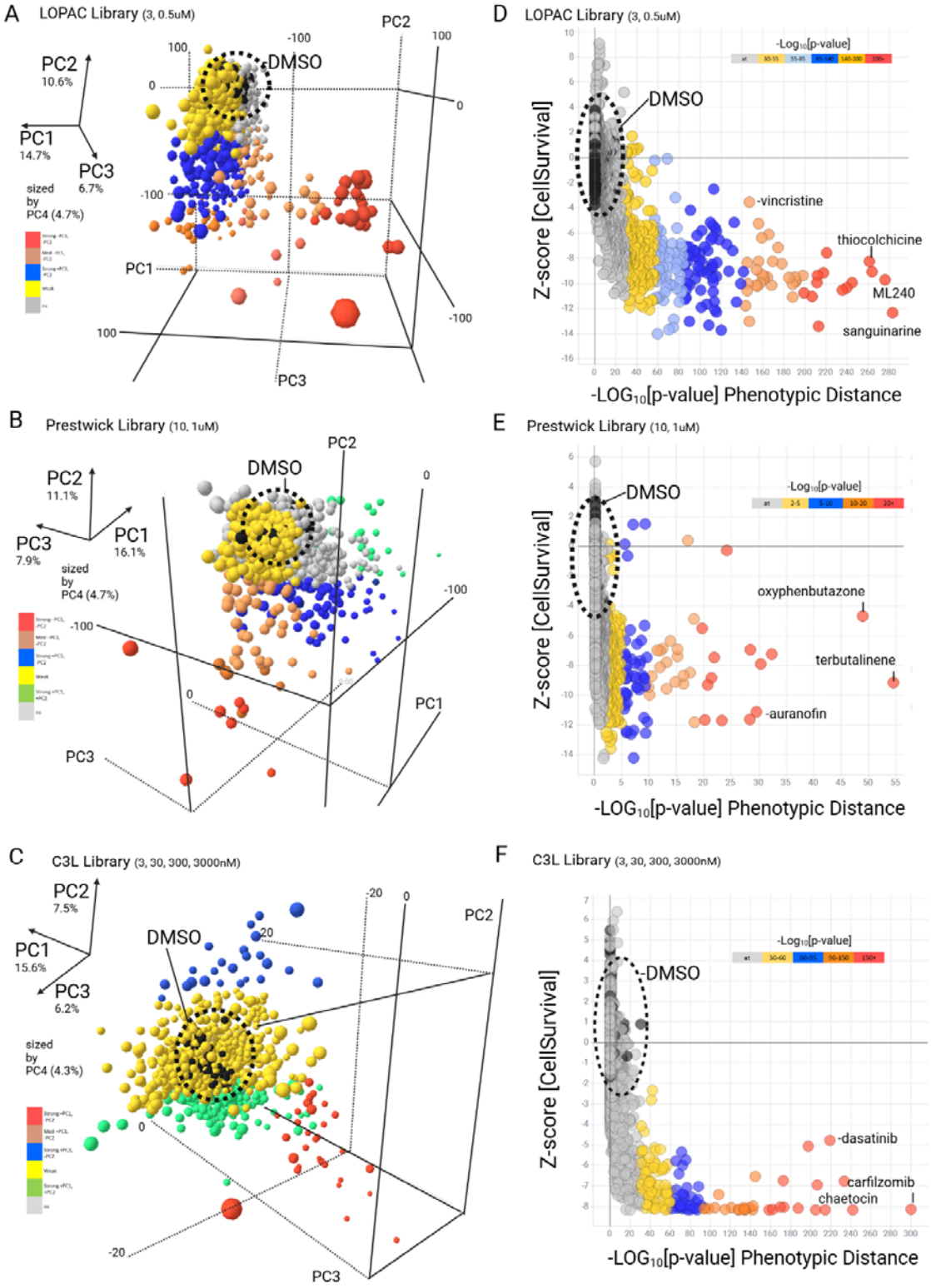

Figure 2. High-content image analysis/dimensionality reduction of drug screening data. A,B,C. Representative data of high content analysis across six GBM stem cell lines and three compound libraries (LOPAC, Prestwick FDA & C3L) by 3D Principal Component Analysis (PCA). DMSO controls circled in Black. Magnitude of vector co-ordinates for PC1,2,3 (sized by PC4) are indicated by colour: Red-pink (strong -PC1, -PC2), Blue (Strong +PC3, -PC2), Green (Strong +PC1, +PC2), Yellow/grey (weaker phenotypes). PC1-4 factor loadings are given (%). D,E,F. Phenotypic distance of screened compounds. We employed 20 principal components (>60% explained variance) to compute a phenotypic distance (Euclidean) for each compound[54]. The corresponding p-values are plotted against cell survival (normalised z-scores, Y-axis). Legend indicates strength of -Log_{10}[p-value] distribution (5 bins, red = maximal effect, reducing to grey where at = arbitrary threshold). Several example hits are labelled.

241 We examined the degree of clustering of compounds with a phenotypic response far from the DMSO
242 controls utilizing a combination of *k*-means clustering and silhouette score analyses (Supplementary
243 Figure 5A,B)[55]. This analysis did not reveal a noticeable cluster structure and thus suggests a lack
244 of morphological or phenotypic diversity of treatment effects across all screened libraries.
245 Additionally, the distribution of the phenotypic distances across individual cell lines and libraries
246 shows substantial heterogeneity in drug sensitivity, with particularly marked differences between
247 the Prestwick and C3L libraries (Supplementary Figure 5C).

248 Initial hit identification was based on two phenotypic criteria, a cell survival threshold (Nuclei Count
249 Z score <-3) and phenotypic distance threshold (negative Log_{10}[*p*-value] >2) capturing changes in cell
250 number and/or morphology following compound treatment in two or more GSC lines. Hit
251 compounds were further triaged by removal of excessive examples of overtly cytotoxic agents
252 (including common anti-cancer agents which have historically been investigated across pan-cancer
253 indications, including GBM), such as microtubule disruptors, topoisomerase poisons and proteasome
254 inhibitors. Compounds active at only high concentration (3µM) were de-prioritised. Short-listed hits
255 were taken forward for further investigation.

256 Two hundred and eleven compounds (8.3% hit rate) were repurchased from different suppliers from
257 that of the original screening libraries, for validation by dose response assay. Fresh compound stocks
258 were prepared in 384-well format in a seven-point semi-log dose response (3-3000nM, 40
259 compounds per plate, with DMSO control wells n= 28). Fresh cell stocks were thawed and the
260 validation protocol was identical to the primary screening assay, with the addition of a normal
261 neuronal stem cell control line (NS69FB_B). Nuclei count data were also extracted from the
262 phenotypic features and the validation set was analysed *via* both multiparametric and univariate
263 analysis, with normalisation to DMSO wells (Figure 3A-C). The multiparametric analysis is presented
264 as -Log_{10}[p-value] Phenotypic Distance across all cell lines (Figure 3A) and we also converted dose
265 response data to normalised Area Under the Curve (nAUC, scaled between 0-1 with 100% death = 0)
266 for validation ranking (nAUC <0.85 in any line) to indicate the potential of achieving a therapeutic
267 window (Figure 3B). Examples of nAUC derived dose response data across each validation plate is
268 shown (Figure 3C) with comparative dose responses between 3 example compounds shown:
269 alisertib (Aurora A kinase inhibitor), OTSSP167 (MELK inhibitor) and APIO-EE-07 (RSK1/MSK2
270 inhibitor) (Figure 3D). In spite of similar dose response profiles between alisertib and OTSSP167,
271 these compounds occupy distinct phenotypic space (Figure 3E and representative images, Figure 3F),
272 hence this approach allowed us to identify compounds with comparable cell survival, while inducing
273 different phenotypic changes *via* distinct MOAs.

274 In this study, validated compound data lists were generated, including separate phenotypic distance
275 and cell survival assay endpoint lists (Table 1 & Supplementary Tables 1 & 2). One hundred and sixty
276 four (164) compounds have been validated in dose response studies (Supplementary Table 1),
277 including 143 compounds originally identified among the 211 hits in the primary screen (68%
278 validation rate) and 21 alternative compounds, selected against target classes represented in the hit
279 list. As expected, there are clear indications of *in vitro* sensitivity of GSCs to topoisomerase poisons,
280 anti-metabolites, proteasome and HDAC inhibitors, as well as particular sensitivity to microtubule
281 targeting agents (taxanes, etc). A prioritized short list (47 compounds) was generated to explore
282 more novel molecular targeted therapies which displayed activity upon GBM and selectivity across a
283 heterogenous GSC panel (Table 1). A network enrichment analysis of this prioritised list was carried
284 out, using the annotated primary protein target(s) for each compound (sources: PubChem, Selleck
285 Chemicals, ChEMBL, canSAR.ai databases), which demonstrates broad coverage of key target linked
286 pathways, including PI3K-AKT, MAPK and EGFR signalling (Figure 3G and Supplementary Figure 6,
287 Supplementary Table 3). Agents of interest involve those targeting cell adhesion (FAK, SRC, YES,
288 FYN), transcription and translation (JAK2/STAT3, CDK9, HDAC, BRD), MAPK pathway/crosstalk
289 (MEK1,2, PAK4,6), DNA damage/repair (TOPO, PARP), mitosis (AURK, KSP), metabolism (FASN,

NAMPT) and protein folding/homeostasis (HSP90, HSF, VCP). There is clear chemical and target diversity within this validated hit list, beyond the expected highly potent cytotoxins, which provides a preliminary shortlist for rational drug-target selection and future systematic drug combination strategies. Any such approach would ideally be compatible with current therapy of post-surgical DNA damaging treatments.

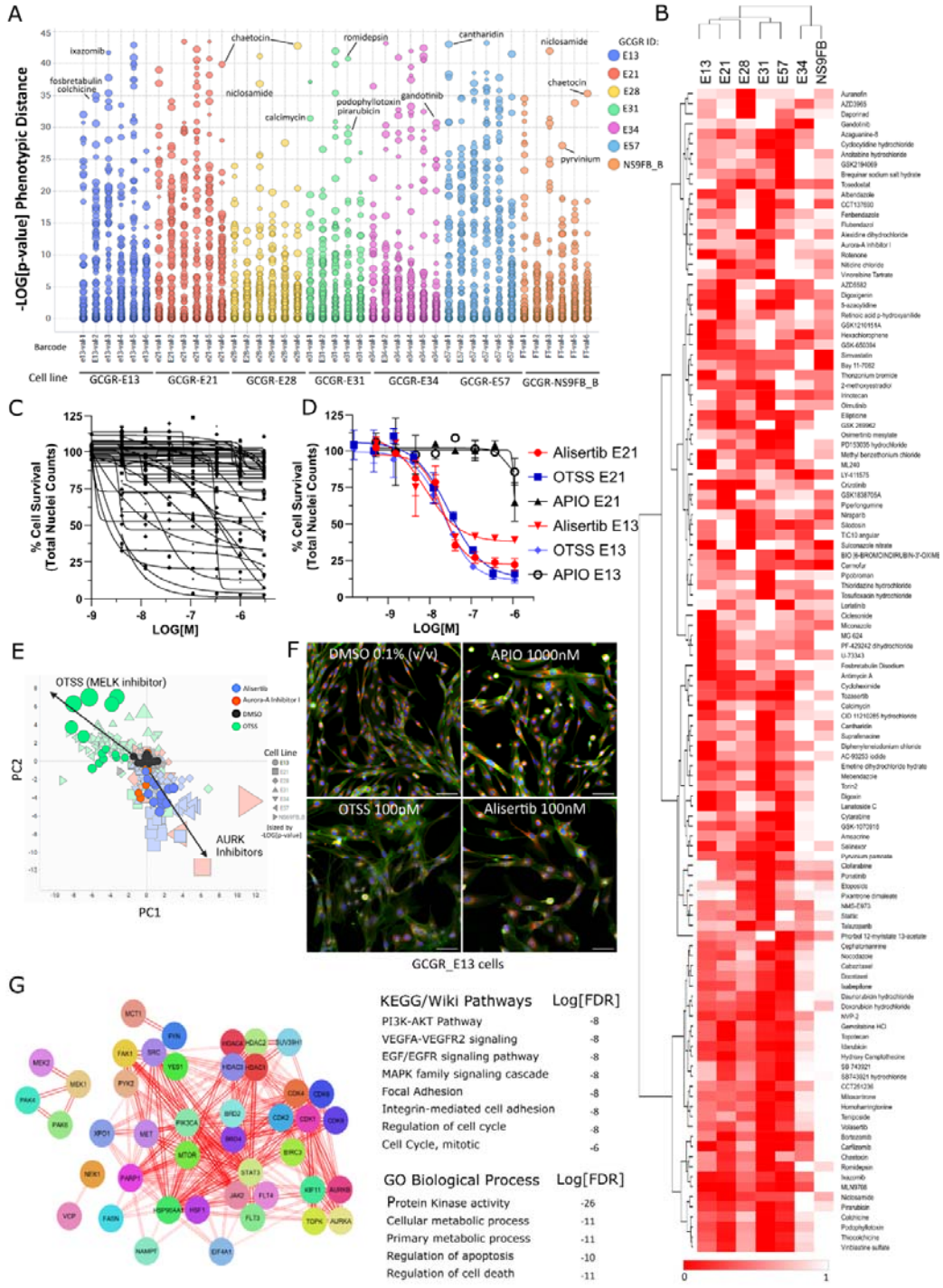

Figure 3. Hit validation from primary screening. A. Scatter plot representing phenotypic distance (negative-Log_{10}[p-value] across 211 compounds and 6 GSC lines and 1 non-transformed NS cells (coloured by cell line, annotated by barcode and sized by dose (~3nM - 1µM). Example hits are labelled. B. Representative heatmap of normalised Area Under the Curve (nAUC) data from dose response data (normalised nuclei counts) across 6 GSC lines and a normal neuronal stem cell control line (NS69FB_B), scaled between 0 (dead) and 1 (100% viable). Potency (low AUC) is indicated in red (relative shading by row). Hierarchical clustering by Euclidean

distance/complete linkage. C. Representative normalised dose response data from a 384w plate (40 compounds per plate, 7 pt dose response, DMSO n=28) used to derive the nAUC. D. Example of dose response validation of alisertib (AURK inhibitor, red) vs OTSSP167 (MELK inhibitor, blue) and relatively inactive compound APIO-EE-07 (RKS/MSK2 inhibitor, black) across E13 and E21 cells. E. Example of distinct principal components/phenotypic space occupied by OTSSP167 (green) vs alisertib (blue) and Aurora A Kinase Inhibitor (red) over multiple doses vs DMSO (black). E13 cells are highlighted (circles) with vector co-ordinates indicated (black arrows). F. Representative images (E13 cells) displaying differing phenotypes between alisertib, OTSSP167 and APIO-EE-07 (vs DMSO) in spite of comparable IC_{50} curves. Staining: (Hoechst (blue), Phalloidin/WGA (green), Endoplasmic reticulum (red). Scale bar 100um. G. STRING-Cytoscape network & enrichment analysis of validated hits, by annotated target(s) search (sources: PubChem, Selleck Chemicals, ChEMBL, canSAR.ai). Lines indicate confidence of molecular interactions (edge score filter 0.4, text mining filter 0.06) with Gene Ontology (GO), KEGG and Wiki terms associated the enrichment analysis, with Log_{10}[False Discovery Rate [FDR] is given. See also Supplementary Table 3.

Compound	Target(s)	IC50 range (6 GBM lines) (nM)	Selectivity/Potency range
Alisertib	AURK	3-20	Broad potency across 6 lines
AZD5582	BIRC3, IAP1/2, XIAP	300	cytostatic, varied
GSK-1324726A (I-BET726)	BRD2/3/4	<100	E21, E57 selective
Dinaciclib	CDK1/2/5/9	10	Broad potency across 6 lines
AZD5438	CDK1/2/9	100-500	Broad potency across 6 lines
Abemaciclib	CDK4/6	200	E21, E57 [mesenchymal] selective
Palbociclib	CDK4/6	100-400	E21, E57, E31 most sensitive
NVP-2	CDK9/cyclinT1	20	Broad potency across 6 lines
AZD4573	CDK9	~20	Broad potency across 6 lines
Foretinib	c-MET, KDR, FLT4	<500	Broad potency across 6 lines
CR-1-31-B	EIF4A	5	Broad potency across 6 lines
POM-HEX	ENOL2/1	100-400	E21, E57 [mesenchymal] selective
Selinexor	exportin-1 (XPO1)	10-200	E28, E31, E57, E13 sensitive
VS-4718	FAK (PTK2), PYK2	1000	E21, E57 [mesenchymal] selective
GSK2194069	FASN [P49327]	1000	Broad potency, cytostatic
CUDC-907 (fimepinostat)	HDAC1/2/3/6/10/11 & PI3K	<100	Broad potency across 6 lines
Emetine	HIF, PDK1, BRD4, ROCK	50-100	Broad potency across 6 lines
NMS-E973	HSP90 (BBB penetrant)	100-300	Broad potency across 6 lines
Gandotinib	JAK2/1, FLT3	100-1000	varied selectivity
SB743921	KIF11 [KSP]	5-10	Broad potency across 6 lines
GDC-0623	MEK1	10-300	E31, E57, E21 selective
Trametinib	MEK1/2	10-300	E31, E57, E21 selective
Gedatolisib/PF-05212384	mTOR, PI3Kα/γ	300	Broad potency across 6 lines
Sapanisertib	mTOR (kinase)	100	E31, E57 sensitive
Daporinad	NAMPT [P43490]	0.250-4	E28, E34, E31 selective
OTS514	NEK1, TOPK --->ERK	20-200	slight E21, E57 selectivity
PF-03758309	PAK4/6 (pan-PAK)	400-600	varied
AZD5305/Saruparib	PARP1	1-10	E28, E34, E31 Long term assays
Niraparib	PARP1/2	130-300	E28, E34, E31 Long term assays
Talazoparib	PARP1/2	1-10	E28, E34, E31 Long term assays
olaparib	PARP1/2	80-300	E28, E34, E31 Long term assays
Rucaparib	PARP1/2	150-300	E28, E34, E31 Long term assays
CCT251236	PIR (HSF1)	300-1000	Broad potency, cytostatic
GSK-1070916	SIK1 [P57059]	300	E57 mostly
AZD3965	SLC16A1 (MCT1)	300	E28, E34 (cytostatic)
Dasatinib	SRC, ABL, c-KIT	<50	E21, E57, E31 most sensitive
Ponatinib	SRC, ABL, PDGFR, VEGFRm FGFR	100-1000	Broad potency across 6 lines
Bosutinib	SRC, ABL, STAT3, ERK	500-1000	Poor potency but distinct phenotype
eCF506	SRC/FYN/YES	30-150	E21, E57, E31 most sensitive
Saracatinib	SRC/FYN/YES	1000	Broad potency across 6 lines
Pyrvinium pamoate	STAT3	<50	E13, E28, E57, E31 sensitive
Chaetocin	SUV39H1/EHMT1	5	Broad potency across 6 lines
NXP-800	HSF-1	500-3500	E63, E55 sensitive
Ganetespib	HSP90	<20	Broad potency across 6 lines
ML240	p97 ATPase	400-1000	E34, E31, E28, E57 sensitive
Pacritinib	JAK2/1, FLT3	1000-2500	E13, E57 sensitive
Niclosamide	STAT3	1000-2000	Broad potency across 6 lines

Table 1. Validated compounds of primary interest. Compounds are listed in alphabetical order of their annotated primary target(s). The IC_{50} range (min to max) across 6 cell lines is given with indicated selectivity between lines (where applicable).

Secondary Assays/Exploration of target classes: Targeting Transcriptional Regulation

As it is beyond the scope of this article to follow up all of these hits in secondary assays, we have provided our full list of validated hit compounds for the GBM research community to explore and perform follow up investigation across similar and alternative GBM models. Within the scope of the current study, we have partially characterised two validated target classes (HDAC and cyclin dependent kinase inhibitors) which demonstrated highly potent (low nM) activity upon GSC survival (Supplementary Table 1).

327 Targeting transcriptional regulation (1): HDAC inhibitors. We further explored a focussed library of
328 54 structurally distinct HDAC inhibitors by dose-response, as our screening data demonstrated the
329 significant potency of this class of compounds across our GSC panel (e.g., romidepsin, panobinostat)
330 (Figure 4). Commercially available HDAC inhibitors were purchased and 384-well dose response
331 plates were prepared and screened against the same six GSC line panel used for primary screening.
332 Compounds were ranked by potency using the cell survival endpoint (normalised nuclei counts)
333 (Figure 4A). Unsurprisingly, the most potent compounds were pan-HDAC or HDAC1/2 inhibitors,
334 although the top ranked compound (with IC_{50} values below 20nM across all cell lines) was the dual
335 HDAC/PI3K inhibitor, fimepinostat (CUDC-907) which is currently undergoing phase II clinical trials in
336 paediatric brain tumours (NCT03893487). Fimepinostat, romidepsin and panobinostat were further
337 validated by performing dose-response and cell cycle analysis (Figure 4B, Supplementary Figure 7A-
338 C). Proliferation/cell survival over 72 hours is non-selectively inhibited across all cell lines, with cell
339 cycle effects generally being limited to either small G_0/G_1 effects or strong G_2/M arrest
340 (Supplementary Figure 7A-C). Live cell imaging on E13 and E57 cells over 96 hours, with an
341 intracellular caspase activity reagent (NucView-488, Biotium), showed a gradual but continuous
342 induction of apoptosis from 24 hours (Figure 4C,D) with corresponding loss of proliferation from 24-
343 36 hours (Figure 4E,F). Staurosporine (STS, 300nM) was used as a positive control for the apoptotic
344 signal.

345 Targeting transcriptional regulation (2): CDK9 inhibitors. Cyclin dependent kinase inhibitors have
346 been extensively investigated for their anti-cancer activity[56, 57] and several CDK inhibitors feature
347 in our validated hit list, including approved CDK4/6 inhibitors abemaciclib and palbociclib. In
348 particular, the CDK1/2/5/9 inhibitor, dinaciclib, as well as the selective CDK9 inhibitor, NVP-2[58],
349 both show potent activity across multiple GSC lines (11-40 nM IC_{50} across the six GSC lines) (Figure
350 5A,B). In addition, a more potent, second generation CDK9 inhibitor, AZD4573, was included in this
351 validation stage and also demonstrated low nM (7-27nM) activity across the 6 GSC lines (Figure
352 5A,B).

353 Dinaciclib is a multi-CDK inhibitor which has gained clinical interest in that it targets both cell cycle
354 progression (*via* CDK1/2) and transcription (*via* CDK9), with this 'dual targeting' mode shown to be
355 effective when combined with cisplatin in ovarian and endometrial cancers[59, 60]. Validation of
356 dinaciclib, NVP-2 and AZD4573 across our GSC panel indicates broad potency at 72 hours across all
357 the cell lines tested (Figure 5A), with G_2/M arrest being initiated at concentrations in excess of 20nM
358 ie below the IC_{50} values observed (Supplementary Figure 7D-F). Live cell imaging of these
359 compounds, on E13 and E57 cells over 96 hours and in the presence of intracellular caspase activity
360 reagent, showed rapid induction of apoptosis beginning at <24 hours from compound addition
361 (Figure 5C,D) with corresponding immediate inhibition of proliferation, as observed from %
362 confluence quantification (Figure 5E,F). Representative images of the phenotypic effects of these
363 compounds at their IC_{50} concentration are shown (Figure 5G). This suggests transcriptional
364 dysregulation *via* CDK9 inhibition is having a significant effect upon cell survival, independent of
365 CDK1/2 inhibition. Overall, AZD4573 has improved cellular potency compared to dinaciclib & NVP-2
366 (Figure 5A,B,G: compare observable 12nM effects vs DMSO).

367

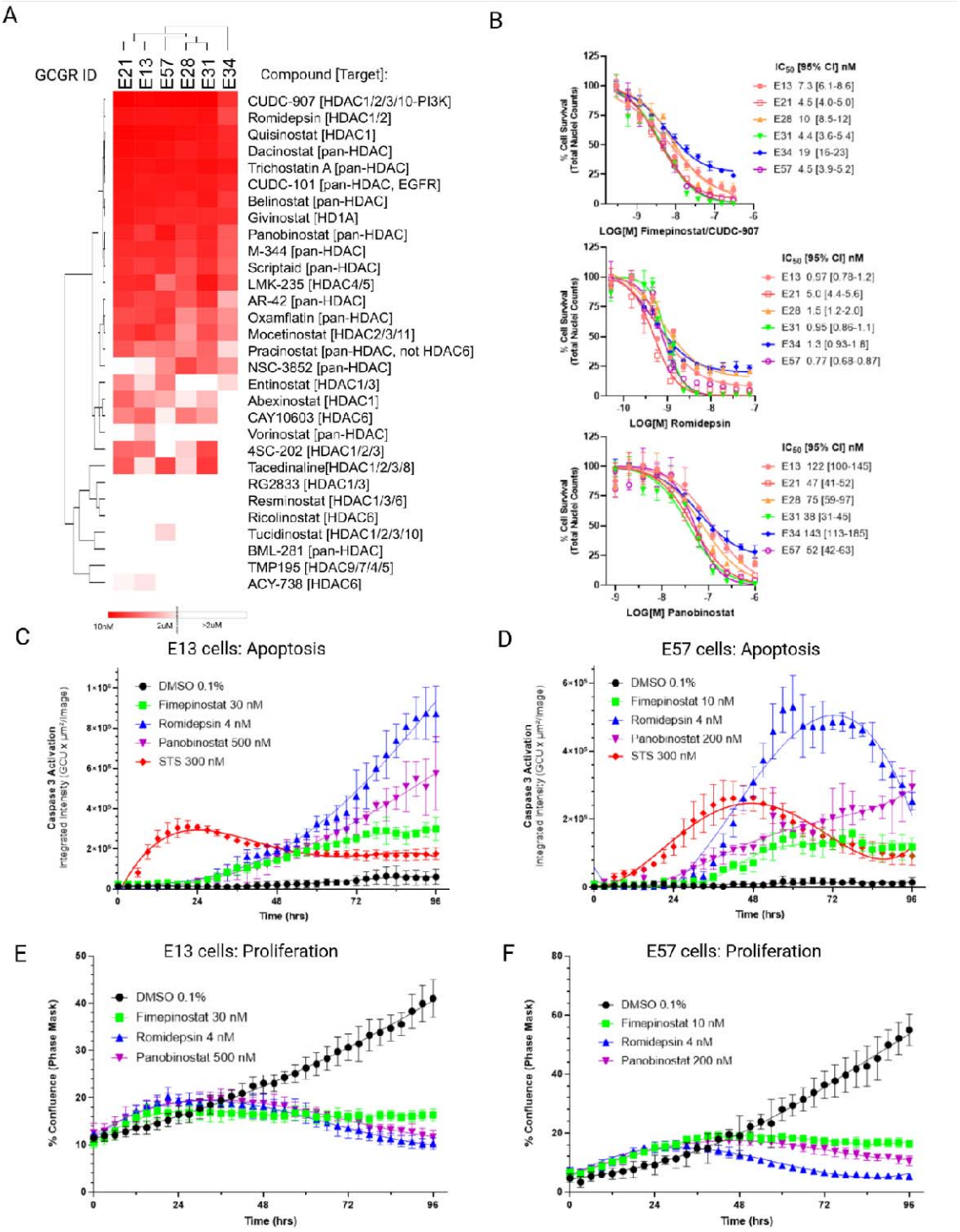

Figure 4. HDAC inhibitor library screening and profiling. A. Representative heatmap of IC_{50} values of HDAC inhibitors on GSC lines, quantified by DMSO normalised nuclei counts at 72 hours. The lowest IC_{50} compounds indicated in red (from 10nM to 2 µM, inactive >2µM indicated in white). Hierarchical clustering by complete linkage, Euclidean distance using Morpheus (https://software.broadinstitute.org/morpheus). B Dose response of fimepinostat (CUDC-907)), romidepsin & panobinostat with indicated IC_{50} values (nanomolar, nM) and 95% Confidence Interval (72 hours, n=3). C&D. Quantification of apoptosis by live cell imaging over time (imaged every 3 hours for 96 hours) at indicated IC_{80} values with staurosporine control (STS, 300nM, red). E & F. Quantification of proliferation over time (imaged at 3-hour intervals for 96 hours), at indicated IC_{80} values. DMSO control (0.1% v/v) is represented in black versus fimepinostat (30nM, green), romidepsin (4nM, blue), panobinostat (500nM, purple).

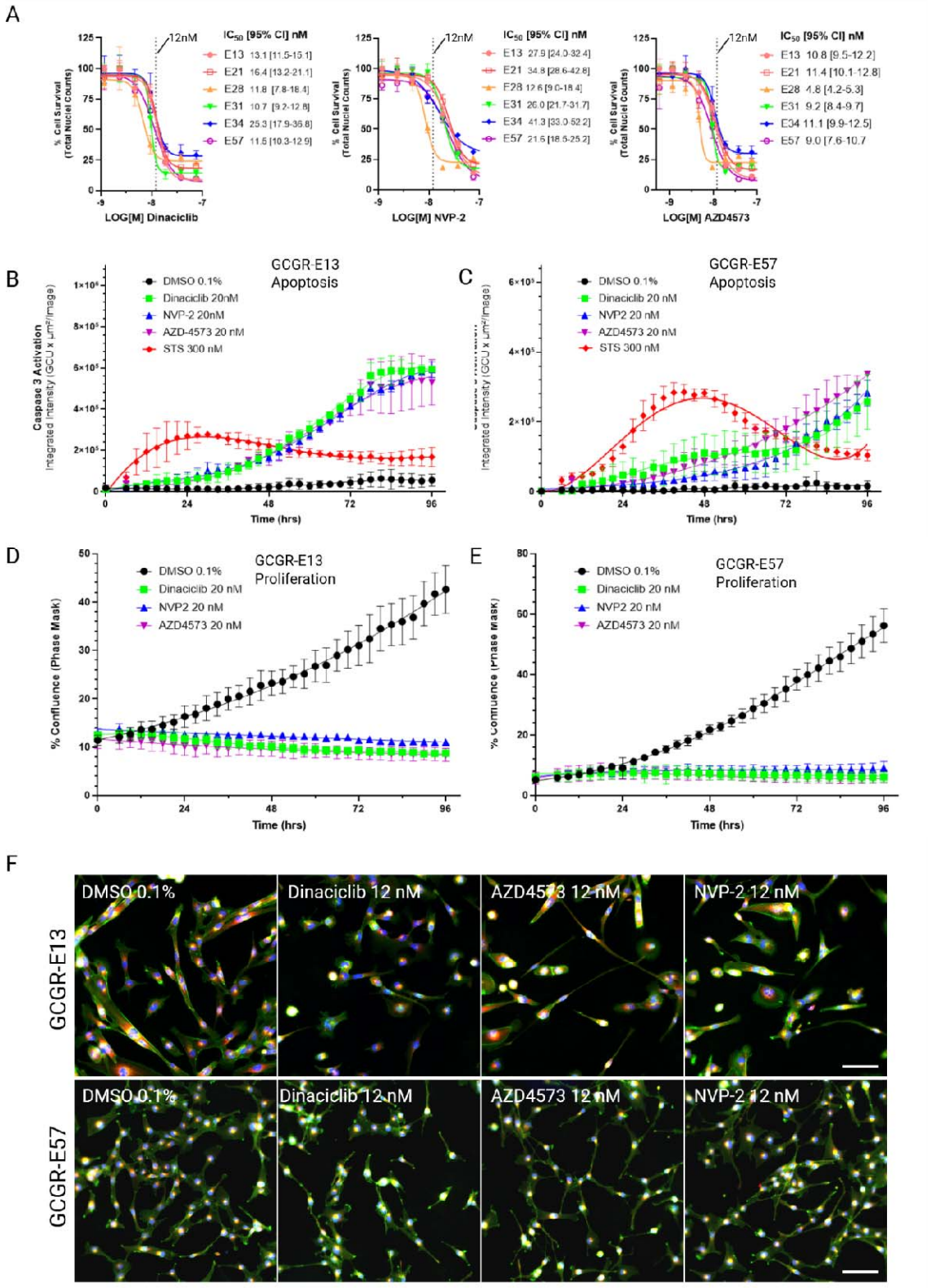

Figure 5. Targeting CDK9 in GBM. A. Dose response validation and IC_{50} values with 95% confidence interval (95% CI) of Dinaciclib, NVP-2 and AZD4573 (n=3). Twelve nanomolar (12nM) concentrations indicated with dotted line. B,C. Quantification of apoptosis by live cell imaging over time (imaged at 3 hour intervals for 96 hours), all compounds at 20nM concentrations with staurosporine control (STS, 300nM, red) and D,E. Quantification of proliferation over time. DMSO control (0.1% v/v) is represented in black, versus dinaciclib (green), NVP-2 (blue), AZD4573 (purple). F. Representative images of Dinaciclib, AZD4573 and NVP-2 at IC_{50} value (12nM) vs DMSO on E57 and E13 cells.

388 From these studies it is clear that targeting HDAC and CDK9, and hence transcriptional regulation,
389 results in a cytotoxic benefit against GSCs, beyond the effects of prolonged cell cycle arrest (with the
390 exception of the highly potent molecule, Romidepsin). To further explore the mechanism of action
391 (MOA) of the CDK9 inhibitors on GSC lines, we performed NanoString™ transcriptomic analysis on
392 E13 cells that were exposed to 20nM of Dinaciclib, AZD4573 and NVP-2, alongside DMSO controls,
393 for 24 hours following compound addition. The extracted mRNA was quantified *via* the nCounter®
394 system (Human Cancer Pathways, 784 genes including controls) and a differential analysis
395 performed. After quality control filtration and removal of housekeeping/control gene sets (post
396 normalisation), 467 genes were available for the differential expression & network pathway analysis,
397 between untreated and treated cells. The results were further filtered by corrected p-value
398 (Benjamini-Yekutieli FDR <0.05) and a minimum 3-fold change. Representative Volcano plots were
399 generated for each compound with some highly significant genes labelled (Figure 6A).

400 Not surprisingly, a large number of genes (168) were significantly dysregulated across all three
401 compounds (Figure 6B), visualised by Venn diagram (Figure 6C). STRING network enrichment
402 analysis (high confidence filter 0.700, no textmining) of these 168 genes (Figure 6D) showed
403 significant enrichment of processes downregulating the MAPK cascade (e.g. *KRAS*, *MAP2K4/MEK4,*
404 *MAPK8/JNK1, MAP2K6/MEK6, DUSP10*), PI3K-AKT signalling (e.g. *PIK3CA/CB/CD* [p100α,β,δ], *IRS1,*
405 *FGFR3, mTOR, MYB*), DNA damage response/repair (e.g. *RAD51, RAD52, BRCA2, PCNA, POLE2*) and
406 apoptotic signalling (Figure 6D. MCL-1, an anti-apoptotic BCL2 family member, is a reported CDK9
407 transcriptional and protein target[61]. This probe is not present in the NanoString™ panel, however,
408 *BCL2* and *BCL2L1* mRNA were downregulated >10 fold, by all three compounds. Very few genes
409 were significantly upregulated for each compound, but notably TSPAN7 (tetraspanin 7) was
410 upregulated 5-8 fold – a protein where low expression is associated with poor prognosis in glioma
411 and negatively correlates with immune infiltration of tumour associated macrophages[62]. The
412 complete network analysis for each compound is provided (Supplementary Figure 8A-I) with
413 enrichment tables and additional data (Supplementary Table 5).

414 Finally, we investigated potential synergistic drug combinations with some of our most potent hits
415 which are currently clinically approved drugs: specifically, dinaciclib against romidepsin (pan-HDAC
416 inhibitor), idarubicin (TOPOII inhibitor) and ixazomib (proteasome inhibitor) (Supplementary Figure
417 9A-O). Querying the Cancer Dependency Map database[63] (depmap.org/portal), a strong 'cell
418 death' correlation was observed between dinaciclib and romidepsin/idarubcin/ixazomib (Supp Fig
419 9B,G,L, R^2 = 0.62 to 0.67) across 564 human cancer cell lines (PRISM Repurposing Public 24Q2
420 dataset). In order to establish if this correlation could predict synergistic interactions, we carried out
421 multiple drug combinations (7x7 dose response matrices) across E13 and E57 cells (72 hours
422 exposure) with quantification from nuclei staining/counts. Whilst the drug combination of dinaciclib
423 with either romidepsin, idarubicin & ixazomib does indicate highly potent additive effects upon GSC
424 survival, synergistic activity was not observed in this instance (Supplementary Figure 9E,J,O).

425

A

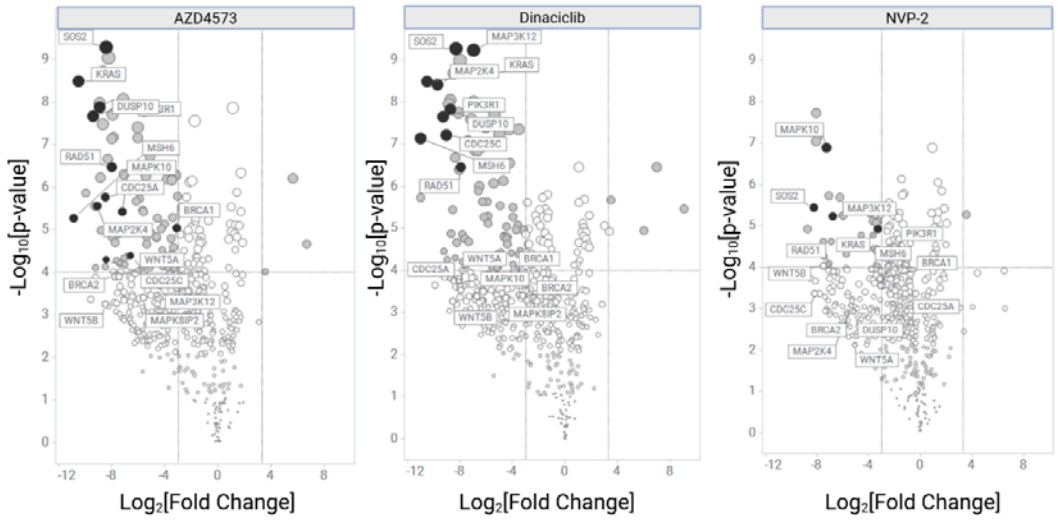

B

AZD4573-NVP2-Dinaciclib:
Significantly downregulated targets

ABL1	FGFR3	PIK3CA
ACVR1B	FST	PIK3R1
ACVR2A	FUT8	PIK3R3
ALKBH2	GAS1	PLAT
ALKBH3	GATA2	PLCB1
AMER1	GHR	PLCE1
APH1B	GSK3B	PLD1
ARID1B	HDAC4	POLB
ARNT2	HDAC5	POLD4
ATR	HIST1H3B	POLE2
AXIN1	HIST1H3G	PPARGC1A
AXIN2	HIST1H3H	PPP3CA
BCL2	IL12A	PPP3CB
BMP2	IL15	PPP3R1
BRCA1	IL22RA1	PRDM1
BRCA2	IL6R	PRKCA
CACNG4	IL7	PRLR
CASP3	IL7R	PTEN
CASP7	IRAK2	PTPRR
CASP9	IRS1	RAD51
CBL	JAK2	RAD52
CCNB1	KDM6A	RAF1
CCNE1	KLF4	RFC4
CDC14B	KRAS	RIN1
CDC25B	LIG4	SHC3
CDC25C	LRP2	SHC4
CDC7	MAML2	SIN3A
CHEK2	MAP2K2	SIRT4
CHUK	MAP2K4	SMAD4
COL2A1	MAP2K6	SMARCB1
CUL1	MAP3K12	SMC3
DDIT3	MAPK10	SOS1
DDIT4	MAPK8	SOS2
DKK1	MDC1	SP1
DTX4	MDM2	SPRY1
DUSP10	MED12	STK11
DUSP5	MEN1	SUV39H2
E2F5	MET	TCF3
EFNA5	MLLT3	TCF7L1
ENDOG	MSH6	TGFB2
EP300	MTOR	TGFB3
ERCC6	MUTYH	TGFBR2
ETS2	MYB	TIAM1
ETV1	NASP	TLR4
ETV4	NBN	TNFRSF10B
ETV7	NSD1	TNFSF10
EYA1	NTHL1	TSC1
FANCA	PAX3	TTK
FANCC	PBRM1	U2AF1
FANCE	PBX3	UBE2T
FANCF	PCNA	VHL
FANCG	PDGFC	WNT5B
FAS	PDGFRA	XPA
FGF11	PHF6	XRCC4

C

B2M
CDKN2A
GADD45B
GNAS
MMP7
TSPAN7 *

AZD4573-NVP2-Dinaciclib:
Significantly upregulated targets

D

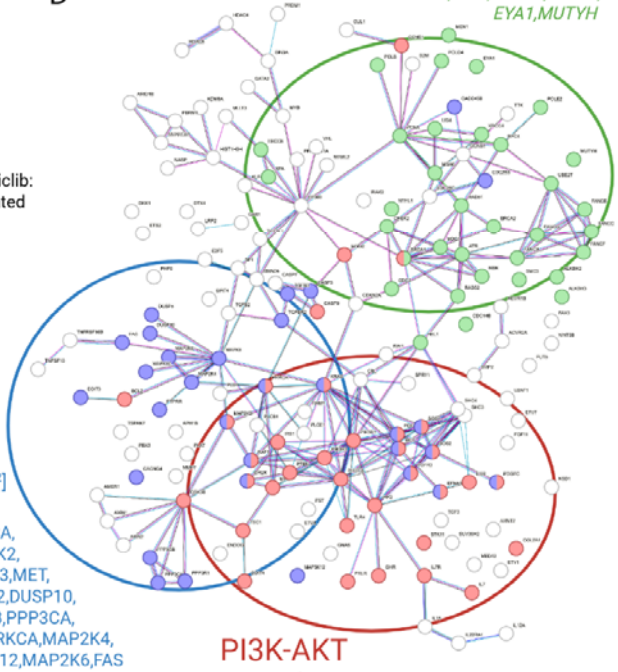

DNA repair/ damage response
GO:0006281 [FDR 10^{-18}]
GO:0006974 [FDR 10^{-24}]

POLE2,NTHL1,FANCE,MSH6, POLB,NBN,FANCC,ALKBH3, POLD4,FANCF,MEN1,ATR, ERCC6,RAD52,SMC3,ABL1, XPA,CDC14B,MDC1,FANCG, PCNA,BRCA2,CHEK2,FANCA, RFC4,CDC7,ALKBH2,BRCA1, XRCC4,LIG4,RAD51,UBE2T, EYA1,MUTYH

MAPK signaling pathway
hsa04010 [FDR 10^{-22}]

PPP3R1,TGFB3, CDC25B,KRAS,PDGFRA, CACNG4,SOS2,MAP2K2, PTPRR,DUSP16,CASP3,MET, EFNA5,FGFR3,TGFBR2,DUSP10, DUSP5,CHUK,PPP3CB,PPP3CA, MAPK8,SOS1,RAF1,PRKCA,MAP2K4, PDGFC,DDIT3,MAP3K12,MAP2K6,FAS

PI3K-AKT signaling
hsa04151
[FDR 10^{-24}]

PIK3CA,SOS2,PDGFRA,MDM2, CCNE1,PIK3R3,MAP2K2,IL7, KRAS,TSC1,IRS1,IL7R,DDIT4, MET,GSK3B,STK11,EFNA5,CASP9, FGFR3,MTOR,IL6R,CHUK,PTEN, TLR4,COL2A1,JAK2,BCL2,SOS1, RAF1,PRKCA,BRCA1,PDGFC,

Figure 6. Differential gene expression (DE) analysis of CDK9 inhibitors on E13 cells from NanoString™ transcriptomics. A. Volcano plots of the differential analysis of E13 cells treated with AZD4573, dinaciclib and NVP-2 (20nM, 24 hrs), relative to DMSO control (0.1% (w/w)). B. Top 168 genes dysregulated by all three compounds (>3 fold change, corrected p-value <0.05). Large panel: downregulated genes, small panel: upregulated genes. TSPAN7 is highlighted with *. C. Venn diagram comparing gene hits across all three compounds. D. Network enrichment analysis (STRING) of top 168 genes. Enriched genes involved in DNA damage and repair (green), MAPK signalling (blue) and PI3K-AKT pathway (red) are highlighted. GO & KEGG terms with FDR is included. Enrichment tables and further data are provided (Supplementary Table 5, Supplementary Figure 8).

DISCUSSION

The clinical treatment of GBM has not significantly improved median patient survival in more than 20 years, with advances in the genomic characterisation of the disease only highlighting the complexity of the clinical challenge. To address this challenge a number of phenotypic screens of drug libraries and drug combinations performed in complex *ex vivo* or *in vitro* GBM models have recently been reported[64, 65]. However, screens reported to date have been limited in terms of the number of compounds, phenotypic endpoints and omission of defined tissue culture conditions which preserve GBM stem cell characteristics. In this study, our aim was to attempt to address the unmet clinical need in GBM by applying a comprehensive target agnostic, high content phenotypic screen, of thousands of compounds across a well characterized panel of patient-derived GBM stem cell models. The drug libraries were selected to support repurposing of existing oncology drug discovery programs and included Phase I passed or FDA/EMA approved small molecules and drugs with high target selectivity across known oncology targets. We have chosen to not exclusively utilise blood-brain-barrier (BBB)/CNS penetrant drug libraries in order to provide a comprehensive and unbiased evaluation of distinct drug and target classes upon GSC phenotypes. It is our hope that this will be informative towards future medicinal chemistry efforts in generating CNS penetrating small molecules against such targets, or possible incorporation of validated hit compounds into emerging blood-brain-barrier penetrating nanoparticles, designed to effectively deliver drugs and drug combinations to GBM [51-53]. In total 3,866 compounds were screened over multiple concentrations, in order to capture the most potent dose-dependent cellular phenotypes beyond simple viability measurements. Our GBM models comprised six heterogeneous, patient-derived GSC lines, representing three of the major transcriptomic subtypes (CLA, MES, PRO). We applied the multiparametric high content 'Cell Painting' assay to screen five drug libraries across the six GSC lines, and provide a validated list of 164 biologically active compounds on human GSC survival and phenotypic activity (Table 1 & Supplementary Tables 1 & 2).

Common cytotoxic agents, such as microtubule targeting agents, topoisomerase poisons, proteasome and HDAC inhibitors, are prevalent in our hit list and many have previously been investigated in GBM (and other cancers). Second generation taxanes, such as cabazitaxel, have shown modest effects with respect to mOS in phase I/II clinical trials (NCT01866449)[66]. The brain penetrant taxane, abeotaxane (TPI-287) showed some promise in phase I trials when combined with bevacizumab (NCT01933815), although confirmation of efficacy *via* phase II trials is required[67]. A recent meta-analysis of the use of the topoisomerase II inhibitor etoposide (44,850 patients over 624 studies published from 1976 to 2011) showed improved median OS (15.66 months vs 13.27, p=0.026) over topoisomerase I inhibitor, irinotecan, which actually showed reduced median OS (10.20 vs 13.55 months, p=0.008). Results are pending for a novel brain penetrant topoisomerase II inhibitor, berubicin (WP744), which has been granted Fast Track Designation by the US Food & Drug Administration[68]. Proteasome inhibitors have been clinically useful in treating blood cancers, such as myeloma[69], unfortunately a phase III study of the brain penetrant proteasome inhibitor, marizomib, did not improve mOS against unstratified patients[70]. The HDAC inhibitor class, such as romidepsin, in general have shown considerable promise as single agents for GBM treatment in the pre-clinical setting, but without translational success[71]. Clinical trials as combination therapy, for example combining panobinostat or vorinostat with radiation, bevacizumab and/or temozolomide have not proved particularly effective[72-74]. Arguably, this lack of clinical success could be

478 attributed to trial design, limited predictive biomarkers, inadequate assessment of brain
479 penetration, etc[75, 76]. Many of these agents have a narrow therapeutic window and significant
480 systemic toxicities limiting their effectiveness. Nevertheless, novel drug delivery technology, such as
481 antibody-cytotoxin conjugates, brain tumour specific nanoparticles[77-79] and intra-cranial drug
482 delivery [80], could still render potent molecules clinically useful in the future.

483 Other molecular targeted compounds identified from our screen, include those targeting cellular
484 adhesion, transcriptional regulation, DNA damage/repair, cell cycle/mitosis/proliferation,
485 metabolism and protein folding/homeostasis, provide a basis for rational drug combination
486 hypotheses and systematic co-inhibition strategies. For example, focal adhesion kinase (FAK) and
487 SRC Family Kinases (SFKs) are downstream effectors of the integrin family of extracellular matrix
488 receptors, and FAK is believed to influence GBM pathogenesis and brain tissue invasion[81-83] while
489 SFKs are recognised drug targets in GBM[84-86] and PYK2 (FAK2)[87], Integrin-Linked Kinase
490 (ILK)[88] and SRC all show high basal expression in our GSC models (Supplementary figure 2).
491 Synergistic drug combinations of FAK or SRC inhibitors with MEK inhibitors have been reported in
492 other cancers[89, 90] and, in a concurrent HTS project, we have found the combination of VS-4718
493 (FAK inhibitor) with trametinib (MEK1/2 inhibitor) to be quite effective in heterogeneous GBM *in*
494 *vivo* models[91]. In fact, recently the combination of the dual RAF/MEK inhibitor Avutometinib with
495 FAK inhibition has been shown to be effective against pre-clinical models of melanoma brain
496 metastases[92]. Also, a phase I/II clinical trial combining avutometinib and defactinib (VS-6063) for
497 $NF1^{del}$ or $BRAF^{mut}$ brain tumours has been initiated (5G-RUBY trial, NCT06630260) while the US Food
498 & Drug Administration has recently granted accelerated approval for the avutometinib/defactinib
499 combination for $KRAS^{mut}$, low grade serous ovarian cancer (RAMP-201, NCT04625270, May 2025).
500 Exploiting GSC vulnerabilities with respect to cellular adhesion and combining with other druggable
501 routes (e.g. EGFR/MAPK/PI3K signalling) remains a viable strategy for GBM treatment. Additionally,
502 we have identified distinct sensitivities to molecules targeting Heat Shock Factor-1 (HSF1;
503 CCT251236, NXP-800), EIF4A (CR-1-31-B), SUV39H1 (chaetocin), FASN (GSK2194069), NAMPT
504 (daporinad), Enolase-2 (POM-HEX), Exportin-1 (selinexor) and JAK2 (gandotinib, pacritinib) (Table 1).
505 Furthermore, our examination of the basal expression of our GSC lines by reverse phase protein and
506 cytokine array also reveals actionable targets *via* high expression of Forkhead Box A1 (FOXA1) and
507 interleukin-8 (IL-8) (Supplementary Figure 2). FOXA1 is usually associated with hormone dependent
508 cancers and can drive endocrine resistance in oestrogen-positive breast cancer[93], or MAPK
509 activation in prostate cancer[94], in an IL-8 dependent manner. Targeting IL-8 *via* humanised anti-IL8
510 antibody[46] is potentially another combination strategy that could be systematically investigated
511 alongside our prioritised hits (Table 1, Supplementary Table 1) .

512 In this article we followed up two drug target classes, HDAC and CDK inhibitors which displayed low
513 nanomolar activity upon inhibiting cell survival across the heterogeneous panel of GSCs. To further
514 explore the HDAC inhibitor class we screened a collection of 54 HDAC inhibitors. Fimepinostat
515 (CUDC-907) was outstanding as the most potent molecule, with <20nM IC_{50} values across the GSC
516 panel. Fimepinostat, a dual PI3K/HDAC inhibitor, is currently undergoing clinical trials for
517 paediatric/young adult brain cancers/solid tumours (NCT03893487), and is potentially a candidate
518 for targeted drug delivery and drug combination strategies. We compared fimepinostat with
519 structurally distinct HDAC inhibitors, romidepsin and panobinostat. While there was a varied cell
520 cycle response between cell lines (Supplementary Figure 7), there was a common intra-cell line
521 response between molecules, suggesting activity is most likely mediated through the anti-HDAC
522 activity of fimepinostat rather than its anti-PI3K activity. Indeed, comparison between fimepinostat
523 and potent, selective PI3K inhibitors (all tested at 30nM) demonstrate substantially weaker activity
524 of PI3K inhibition upon GSC proliferation, with only dual PI3K/mTOR inhibitor, gedatolisib (PF-
525 05212384), showing any significant effect (Supplementary Figure 10). While the lack of success in
526 targeting GBM with PI3K monotherapy may indicate a lack of true oncogenic addiction to PI3K

signalling, drug combinations with PI3K/mTOR/AKT inhibitors are still viable options against PTEN deficient, GBM tumours[95].

Targeting transcriptional regulation has previously been shown to be effective against cancer stem cells (including brain cancers)[96-98], hence we also characterised potent CDK9 inhibitors dinaciclib, NVP-2 (both screening hits) and a more recent selective CDK9 inhibitor, AZD4573. CDK9 is an atypical CDK in that it is a key regulator of RNA Polymerase II (Pol II) transcription initiation, elongation and termination, playing a critical role in transcriptional regulation[99]. Dinaciclib has near equal potency against CDK1/2 (& 5), whereas NVP-2 and AZD4573 are classed as CDK9 selective[100, 101]. AZD4573 has progressed to clinical trials (NCT04630756) and is well tolerated, although CNS penetrance and solid tumour efficacy remains to be determined. Radiosensitisation of cancer cells with CDK9 inhibitors and drug combinations with DNA damaging agents have previously been reported[102-104], including opportunities in GBM[105]. In our *in vitro* assays, dinaciclib, NVP-2 and AZD4573 are highly potent across all GSC lines tested, being strongly antiproliferative with predominant G_2/M arrest and induction of apoptosis. Differential gene expression analysis of GSC cells exposed to CDK9 inhibitors, reveals highly significant decreases in the expression of genes regulating the cell cycle, DNA damage and repair, anti-apoptosis, PI3K and MAPK signalling (Figure 6, Supplementary Figure 8, Supplementary Table 5). It is noteworthy that, of the very few genes upregulated in response to CDK9 inhibition, Tetraspanin-7 (TSPAN7/TM4SF2) expression is increased 5-8 fold (Figure 6B). An increase in TSPAN7 expression in GBM is associated with improved prognosis and immunosuppression of the tumour microenvironment[62], potentially impacting GBM response to anti-PD1 or anti-PD-L1 immunotherapy when also combined with CDK9 inhibition. These results indicate that the CDK inhibitors are reprogramming the GSCs into a more vulnerable state, leading to inhibition of cell survival and, together with previous publications implicating CDK9 as a therapeutic target in GBM[105], suggest targeting CDK9 is worth further exploration in other GBM models and with other drug combinations.

Overall, our screening results presented here serve as a foundation for a systematic approach to the identification, validation and prioritisation of novel therapeutic strategies in GBM including future drug combinations, that could be used concurrently or following standard treatment protocols for GBM. Importantly, we have used patient-derived GSC models, grown under stem-like conditions on a laminin rich ECM scaffold to prioritize follow up investigations of highly potent small molecules active across a genetically distinct and heterogeneous GSC panel. The objective of our phenotypic screening assay was to identify multiple drug targets and mechanisms-of-action which target heterogeneous GSC phenotypes and thus complements the existing focus on known oncogenic drivers that represent established drug target classes. We anticipate that this approach will identify new therapeutic targets and drug combination hypotheses that target GSC phenotypes rather than individual pathways and thus may be more resilient across heterogeneous patient populations and adaptive drug resistance mechanisms.

In conclusion, our high content screening followed by multi-cell line validation across primary and secondary phenotypic assays provides the largest unbiased survey of small molecule therapeutic classes and oncology targets upon GBM stem cell phenotypes that we are aware of. We provide our full list of validated hits active upon GBM stem cell morphology and cell survival for the research community to explore further. Future studies include expanded screening across larger target-annotated and diverse chemical libraries to identify novel chemical starting points and novel targets for new GBM drug discovery programs. In addition, further profiling of phenotypic screening hits across a larger number of GBM stem cells lines and integration of phenotypic with molecular data, in order to identify synthetic lethality relationships and/or predictive biomarkers of response, will support additional personalized medicine strategies for both existing and new drug target classes in GBM. Importantly this unbiased approach can identify new therapeutic opportunities for the

576 majority of GBM patients which do not fall into well-defined subtypes characterized by well-known
577 druggable driver genes thus expanding the scope and inclusion criteria of personalized medicine
578 strategies in GBM.

579

580 ACKNOWLEDGEMENTS

581 This work was funded by a joint Cancer Research UK (C42454/A28596) and The Brain Tumour Charity
582 award (GN-000676) to D.E., N.O.C. and M.C.F. G.M.M and the Glioma Cellular Genetics Resource
583 (gcgr@ed.ac.uk) were supported by the Cancer Research UK (CRUK) Centre Accelerator Award
584 (A21922).

585 CONFLICTS OF INTEREST

586 S.P. is a co-founder, shareholder and Chief Scientific Officer of Trogenix Ltd.

587 N.O.C. is a co-founder, shareholder and management consultant for PhenoTherapeutics Ltd.

588 N.O.C and M.C.F have held advisory positions and are shareholders in Amplia Therapeutics Ltd.

589 N.O.C. had patents pertaining to discovery of the SRC/YES1 inhibitor, eCF506/NXP900 (
590 EP3298015B1, JP6684831B2, US10294227B2, CN107849050B, and CA3021550A1) licensed to
591 Nuvectis Pharma and has received grant funding from Nuvectis Pharma.

592 FUNDING

593 This work was supported by a Cancer Research UK/Brain Tumour Charity grant C42454/A28596.

594

Materials and Methods

Cell culture

Cell lines were obtained from the Glioma Cellular Genetics Resource, Edinburgh (gcgr@ed.ac.uk, https://github.com/GCGR) and cultured according to optimised conditions for glioma stem cell growth (gcgr.org.uk). Briefly, cells were cultured in DMEM/HAMS-F12 media (Merck, D8437) with B27, N2 supplements (GIBCO 17504-044, 17502-048), EGF/FGF (10ng/mL, Peprotech 315-09, 100-18b)), glucose (8mM, Merck, G8644), MEM non-essential amin acids (5mL, GIBCO 11140-035, 100X), BSA (0.012%, GIBCO 15260-037), β-mercaptoethanol (0.1mM, GIBCO 31350-010) and laminin (4-10µg/mL depending on the cell line, Cultrex 3446-005-01). Cells were passaged at ~80% confluence (4-7 days) and dissociated using Accutase (Merck, A6964) . Doubling times are approximately 60 hours (except E57 cells, doubling time ~24 hours) with generally low passage ratios (1:3 to 1:6) to maintain no less than 20% confluence during cell expansion. Cell lines were submitted for STR profiling (ECACC, case number 21579, using a Promega Powerplex 16 HS kit) and were routinely monitored for mycoplasma infection (MycoAlert®, Lonza). All cell lines were expanded and banked in liquid nitrogen (~24 vials each) for continuous turnover of low passage lines during screening.

Compound screening

384-well plates (Greiner Bio-One, µClear, 781091) were precoated in growth media containing 10ug/mL laminin (20µL/well) and incubated for 2 hours at 37 °C, 5% CO_2 (minimum). Single cell suspensions in growth media were prepared (final seeding densities indicated in Supp Figure 1B) and added to the pre-coated plates (30µl/well, final laminin 4µg/mL). The plates were then incubated for ~20 hours and inspected briefly, prior to compound addition using a Biomek automated liquid handler. Compound library plates (as assay ready daughter plates in 100% dimethylsulfoxide (DMSO), 10mM-1mM stocks, prepared *via* BioAscent compound management (bioascent.com)) were diluted with media to intermediate plates (1:50, 2% DMSO (v/v)) prior to addition to cells (1:20, final 0.1% DMSO (v/v)). Where required, the intermediate drug plates were further diluted to create reduced dose intermediate plates (with 2% DMSO (v/v)) prior to addition to cells (1:20, final 0.1% DMSO (v/v)). Negative controls (DMSO, 0.1% (v/v), n= 32-48 per plate) and positive controls (staurosporine, 1µM final conc., n= 16) for cell death were added to the intermediate compound plates (up to 320 compounds per plate). After the addition of compounds, the plates were then incubated at 37 °C, 5% CO_2 for 72 hours. Compound resupply details are provided in Supplementary Table 4.

Table 2: Screening libraries and concentrations used

Library	# Compounds	Source	Concentrations Used (nM)	Controls (nM)
TargetMol-Anti-Cancer	330	TargetMol #L2110 (2018)	10000, 100, 10, 1nM	Paclitaxel (5nM), Staurosporine (100 nM)
Kinase Chemogenomic Set (KCGS)	187	Structural Genomics Consortium https://cancertools.org/the-kinase-chemogenomic-set-kcgs/	1000, 100 nM	Paclitaxel (5nM), Staurosporine (100 nM)
Prestwick FDA	1280	Prestwick Chemical (~2016) https://www.prestwickchemical.com/screening-libraries/prestwick-chemical-library/	10000, 1000 nM	Staurosporine (1000nM)
LOPAC® (Library of Pharmacologically Active Compounds)	1280	Merck/Sigma-Aldrich (LO4100)	3000, 500 nM	Staurosporine (1000nM)
Comprehensive Anti-Cancer Compound Set C3L	789	Custom (reference 53; Athanasiadis et al, 2023)	3000, 300, 30, 3 nM	Staurosporine (1000nM)

629

630 Cell painting

631 Live mitochondrial staining of cells was carried out by the addition of MitoTracker Deep-Red solution
632 (3µM, 10X conc. in media at 5µL/well) using the Integra Viafill automated dispenser (Intergra
633 Biosciences). The plates were then incubated for 30 minutes at 37 °C, 5% CO_2 followed by plate
634 cooling and fixation by the addition of 15% formaldehyde in phosphate buffered saline (PBS)
635 (20uL/well – final 4% formaldehyde in 75µL volume) using a multidrop combi reagent dispenser.
636 After incubation for 20 minutes, the plates were washed (BioTek plate washer, Agilent,
637 www.biotek.uk.com) with PBS and cell painting reagents prepared in 1% BSA/0.01% TX-100 in PBS
638 (Table 3). After washing, PBS was removed and cell painting solution was added using a multidrop
639 combi (20µL/well) followed by incubation at room temperature for 30 minutes. The staining solution
640 was then removed, the plates washed with PBS, sealed (Starseal foil seals, Starlab, E2796-9792)
641 then imaged immediately.

642 **Table 3. Cell painting reagents listed by target organelle, channel, final concentration & supplier**
643 **details.**

Stain	Structure	Wavelength, ex/em (nm)	Channel	Final Concentration	Catalogue No., Supplier
Hoechst 33342	Nuclei	387/447	DAPI	5µg/mL	H1399, Molecular Probes
Concanavalin A Alexa Fluor 488	Endoplasmic reticulum	462/520	FITC	33µg/mL	C11252, Invitrogen
SYTO 14	Nucleoli	531/593	CY3	3 µM	S7576, Invitrogen
Phalloidin Alexa Fluor 594	F-actin	562/624	TxRED	7U/mL (1:1500)	ab176757, Abcam
Wheat germ agglutinin Alexa Fluor 594	Golgi and plasma membrane	562/624	TxRED	3µg/mL	W11262, Invitrogen
MitoTracker DeepRed	Mitochondria	628/692	CY5	300nM	M22426; Invitrogen

644

645 Image acquisition

646 Images were acquired using ImageXpress Confocal HT.ai high content microscope (Molecular
647 Devices LLC, version 6.5.0) with automated plate handling (GX series, Peak Analysis and
648 Automation). Exposure settings for each channel were optimised and set for screening. Each well
649 was imaged using a 20× objective and 6 fields of view (30 images per well over 5 channels, ~33% well
650 coverage, typically 75-150 cells per image)

651 Image analysis, quantification and data processing/plotting

652 CellProfiler v3.1.5 image analysis software (cellprofiler.org) was used to create a custom analysis
653 pipeline across 5 channels capturing 1155 features per cell (processed features & factor
654 loadings/explained variance is provided in Supplementary Table 5). Images were analysed *via*
655 parallel processing using a Unix/Linux high performance computing cluster (University of Edinburgh)
656 and concatenated outputs included median aggregated, well level data. Each completed dataset
657 (library across 6x GCGR lines) was then batch processed using StratoMineR high content analysis
658 platform (stratominer.com). Briefly, stepwise processing in StratoMineR included metadata
659 integration, removal of redundant features (correlation cut-off 0.99, typically 800-850 features
660 remaining), QC and control annotation/flags, normalisation (to DMSO and sample wells, on a plate-
661 by-plate basis), transformation (Skewness significance 0.0001), feature scaling (robust z score, by
662 plate) and dimensionality reduction (principal component analysis [generalised weighted least
663 squares], Oblique rotation, Ten Berge factor scores method, auto correlation cut-off with ≥20 factors
664 chosen [model based on samples] to represent >60% of data variance [Scree plots]) and
665 computation of phenotypic distance/p-values from principal component vectors[54].

666 Processed data was then exported and analysed further using TIBCO Spotfire analysis software
667 (spotfire.com), including plot generation. Hierarchical clustering of normalised datasets was carried
668 out using Morpheus (https://software.broadinstitute.org/morpheus) by complete linkage, Euclidean

669 distance). Network and enrichment analysis of top ~50 [supplier] annotated compound targets was
670 carried out using STRING[106] & CytoScape (cytoscape.org)[107]. Cell cycle analysis was carried out
671 from DNA content/nuclei images (Hoechst stain) using MetaXpress software (Molecular Devices LLC,
672 version 6.5.0). Dose response data and curve fitting (non-linear regression) was carried out using
673 GraphPad Prism (version 7.05). Synergy plots were generated using SynergyFinder+ web
674 application[108] (https://synergyfinder.org/)

675 Clustering Analysis and distribution plots

676 To quantify the phenotypic diversity of the screened compounds with z-score[cell survival] < -3 and -
677 Log_{10}[*p*-value] >2 we performed *k*-means clustering of the unique 245 compounds that passed this
678 threshold using the principal components derived from the morphological features (20 PCs for
679 libraries LOPAC and Prestwick; 10 PCs for C3L library). The degree of clustering was quantified by the
680 *k*-means score defined as the within-cluster sums of point-to-centroid distances, summed across all
681 clusters. The quality of the *k*-means clusters was determined with the silhouette coefficient *S*
682 averaged across the unique compounds per library[55]. The silhouette coefficient varies between −1
683 and 1, with $S=1$ indicating that compounds are in well separated clusters, $S=0$ indicating
684 overlapping clusters, and $S=-1$ indicating incorrect assignment of clusters. The distribution of the
685 variable -Log_{10}[*p*-value]. Phenotypic Distance was calculated using violin plots per cell per library.
686 These measures were calculated using R version 2023.9.0.463 with libraries base stats (function
687 kmeans), cluster_2.1.4 (function silhouette) and ggplot2_3.4.3 (function geom_violin).

688 Live Cell Imaging/Apoptosis Assays

689 GCGR-E13 (1000 cells/well) and GCGR-E57 cells (500 cells/well) were seeded (45µL/well) onto 384-
690 well plates (Greiner uClear, 781910) pre-coated with 10µg/mL Laminin ECM. After overnight
691 incubation, a solution of NucView-488 reagent (10X conc., 50µM) was added using an Integra ViaFill
692 Liquid dispenser (5µL/well). The compounds were then immediately added using a D300e
693 nanodispenser with back-filling of DMSO to 0.1% (v/v) for all wells, triplicate wells per dose (3
694 concentrations per compound, based on individual IC50 range). Staurosporine (300nM, 6 replicates
695 per cell line) was used as a positive control for apoptosis induction against DMSO controls (0.1%, 6
696 replicates per cell line). The plate was then loaded into an IncuCyte S5 Live Cell imager with scans set
697 at 3-hour intervals for 96 hours (phase and 'green' channels, 10× objective, 1 site). Image processing
698 was carried using IncuCyte in-built analysis modules, with phase area defined as %
699 Confluence/image from the first scan (~t = 0+30mins). Apoptosis was quantified from images
700 showing increasing Integrated Intensity from the NucView-488 emission signal (GCU x μm^2/Image).

701 NanoString™ sequencing/differential analysis

702 mRNA was extracted from E13 cells (~$3x10^6$ cells each condition) after 24 hours treatment with
703 AZD473, Dinaciclib, NVP-2 (all 20nM) & DMSO (0.1% v/v) in triplicate 10cm dishes, using RNeasy Plus
704 miniprep extraction kit (Qiagen, #74134). Purified mRNA was quantified and diluted to 20ng/uL and
705 submitted for NanoString™ nCounter® analysis against the Human Cancer Pathways Panel
706 (NS_CancerPath_C2535). Samples were hybridised and immediately processed using the nCounter®
707 Prep Station and Digital Analyzer (High Sensitivity protocol). QC checks utilised GeNorm to
708 determine most stable reference genes and no QC Flags were raised overall. Differential analysis was
709 carried out on normalised data (normalised to ~20 housekeeping genes) using nSolver™ Analysis
710 Software (version 4.0.70) following standard analysis pipelines. Exported data was replotted using
711 TIBCO Spotfire software and also further analysed by hierarchical clustering
712 (https://software.broadinstitute.org/morpheus) and STRING network analysis (string-db.org)[106].
713 Venn diagrams were generated from Molbiotools (molbiotools.com/listcompare.php)

714 Forward-phase protein array: basal cytokine analysis.

715 Conditioned medium was collected after 72 hours incubation. Microarrays were generated using an
716 in-house Aushon BioSystems 2470 array printing platform. The arrays were blocked for 1 hour with
717 Superblock T20 Blocking Buffer (Grace Bio Labs) at room temperature. Conditioned media from
718 glioma stem cell samples were centrifuged at 1000× *g* for 5 minutes at 4 °C. Supernatants were
719 collected and added to microarrays followed by incubation overnight at 4 °C. The arrays were

720 washed three times for 5 minutes in PBS-T (PBS-Tween 0.1% v/v) and blocked for 10 minutes with
721 Super G Blocking Buffer at room temperature on a rocking platform, then washed again washed
722 three times for 5 minutes in PBS-T. Detection antibody mixtures (1:500 antibody dilutions in 5%
723 bovine serum albumin/phosphate buffered saline tween-20 0.1% (BSA/PBS-T), 10% Super G Blocking
724 Buffer) were made in microplates. Microarrays were clamped and 50 µL of each antibody was added
725 to corresponding microarray wells. Microarrays were incubated for 1 hour on a rocking platform.
726 Clamps were removed and microarrays were washed three times for 5 minutes in PBS-T. Microarrays
727 were then blocked for 10min with Super G Blocking Buffer at room temperature and again washed
728 three times for 5 minutes in PBS-T. Three millilitres (3 mL) of IRDye 800CW Streptavidin (LI-COR
729 Biosciences) was diluted 1:5000 in PBS-T supplemented with 5% BSA, 10% SuperG Blocking Buffer.
730 Microarrays were covered and incubated with IRDye on a rocker at room temperature for 30
731 minutes, then washed for 5 minutes, three times in PBS-T followed by three 5-minute PBS washes
732 and finally washed with distilled water. Microarrays were dried then scanned at 795nm on the
733 InnoScan 710 high-resolution microarray scanner (Innopsys Life Sciences). The data was normalised
734 for protein concentration and background fluorescence *via* Microsoft Excel templates.

735 Reverse-Phase Protein Array (RPPA): Basal analysis

736 GSC lines were cultured both as mono-layers on laminin-coated cell culture plates and as spheroid
737 cultures on poly-hema coated plates. Cells were set up as mono-layer and spheroid cultures in
738 parallel by seeding equivalent cell numbers from a parental flask with cells in log-phase growth.
739 Cultures were grown until the mono-layer cultures were approximately 70% confluent and then both
740 adherent and suspension cultures were harvested for lysis and preparation for RPPA. For Laminin
741 coating, plates were incubated with Laminin at 10ug/ml for 1 hour and then washed with PBS prior
742 to addition of cell lines. Culture media did not contain Laminin and the same media was used for
743 adherent and suspension cultures. For Poly-hema coating plastic 2.4g of poly-hema was dissolved in
744 200ml of 95% Ethanol and heated to dissolve. The solution was centrifuged at 2500RPM to remove
745 undissolved particles. 4ml was added per 10cm plate (ensuring the plate was completely coated).
746 Plates were left open in a TC hood to air-dry and were rinsed x3 with PBS prior to addition of cells.

747 Mono-layer cultures were washed twice with PBS after removal of media and snap frozen on dry-ice
748 and stored at -80°C. Spheroid cultures were pelleted by centrifugation and washed twice with PBS
749 and then snap frozen and stored until lysis. Cultures were lysed in RIPA buffer supplemented with
750 ROCHE PhosStop and cOmplete Mini inhibitor tablets (Merck, 04906845001 & 11836153001).
751 Lysates were needle syringed five times to ensure complete lysis of cells. Protein quantification was
752 carried out using Coomassie-plus assay (ThermoFisher #23228) and protein concentration was
753 adjusted by to 1 mg/ml. Samples were prepared for printing by addition of 4x Sample buffer and
754 heat denaturation at 95°C for 5 minutes.

755 All samples were diluted to 0.75mg/ml (D1), 0.375mg/ml (D2), 0.1875mg/ml (D3) and 0.09375mg/ml
756 (D4) using PBS containing 10% Glycerol. Array spotting was carried out with the Quanterix 2470
757 Arrayer platform using 185µM pins. Each sample was spotted at four dilutions (D1-D4) onto single
758 pad ONCYTE® SuperNOVA nitrocellulose slides at a 500µM spot-to-spot distance. 268 signalling
759 pathway markers (and appropriate controls) were profiled in a standard RPPA assay as described
760 briefly below. After spotting, the slides were incubated with antigen retrieval solution (1x Reblot
761 strong) for 10 mins before being placed in a microfluidic structure to individually address the arrays
762 with primary or secondary antibody solutions. Following blocking buffer (Superblock T20) for 10
763 mins the detection of marker antibodies was performed in a two-step sequential assay (1)
764 incubation of an array with primary analyte-specific antibody in blocking buffer for 60 mins at room
765 temperature and (2) removal of excess antibody by washing arrays with PBS-T, followed by a further
766 incubation with blocking buffer and PBS-T washes, and incubation secondary antibody (Dylight-800-
767 labeled anti-species antibodies diluted 1:2500 in Superblock T20) for 30 mins. After further washing
768 and slide drying, the arrays were imaged in the Innopsys Innoscan 710 scanner. Blank signals were
769 determined by omitting the primary antibody from step 1 and instead incubating the array with
770 Superblock T20 alone, followed by step 2. Sample loading on arrays (for normalisation) was
771 determined by staining one slide with fast green protein dye and scanning at 795nm. Microarray
772 images are analyzed using Mapix software (Innopsys). The feature (spot) diameter of the grid was

773 set to 270µm. The average signal intensity is determined for each individual feature and the median
774 background from the adjacent area is subtracted from each feature signal leading to a net signal per
775 feature. Data analysis is performed in a standard way: Fluorescence intensity for each feature on the
776 array is measured. A test is performed for linear fit through the 4 point dilution series for all samples
777 on all arrays using a flag system where R2 > 0.9 (green flag) is deemed good, >0.8 (amber flag) is
778 deemed acceptable and <0.8 (red flag) is poor and may be excluded from data analysis. The median
779 values from the 4 point dilution series are calculated and used as a measure of fluorescence
780 intensity. Data is quantified as RFI (relative fluorescence intensity) values relating to relative
781 abundance of total and phosphorylated proteins across the sample set.

782

783 References:

784

785 1. Philips, A., et al., *Brain Tumours: Rise in Glioblastoma Multiforme Incidence in England 1995-*
786 *2015 Suggests an Adverse Environmental or Lifestyle Factor.* J Environ Public Health, 2018.
787 **2018**: p. 7910754.
788 2. Stupp, R., et al., *Radiotherapy plus concomitant and adjuvant temozolomide for*
789 *glioblastoma.* N Engl J Med, 2005. **352**(10): p. 987-96.
790 3. Dolecek, T.A., et al., *CBTRUS statistical report: primary brain and central nervous system*
791 *tumors diagnosed in the United States in 2005-2009.* Neuro Oncol, 2012. **14 Suppl 5**(Suppl
792 5): p. v1-49.
793 4. Lan, Z., X. Li, and X. Zhang, *Glioblastoma: An Update in Pathology, Molecular Mechanisms*
794 *and Biomarkers.* Int J Mol Sci, 2024. **25**(5).
795 5. Noroxe, D.S., H.S. Poulsen, and U. Lassen, *Hallmarks of glioblastoma: a systematic review.*
796 ESMO Open, 2016. **1**(6): p. e000144.
797 6. Verhaak, R.G., et al., *Integrated genomic analysis identifies clinically relevant subtypes of*
798 *glioblastoma characterized by abnormalities in PDGFRA, IDH1, EGFR, and NF1.* Cancer Cell,
799 2010. **17**(1): p. 98-110.
800 7. Brennan, C.W., et al., *The somatic genomic landscape of glioblastoma.* Cell, 2013. **155**(2): p.
801 462-77.
802 8. Singh, S.K., et al., *Identification of a cancer stem cell in human brain tumors.* Cancer Res,
803 2003. **63**(18): p. 5821-8.
804 9. Singh, S.K., et al., *Identification of human brain tumour initiating cells.* Nature, 2004.
805 **432**(7015): p. 396-401.
806 10. Hemmati, H.D., et al., *Cancerous stem cells can arise from pediatric brain tumors.* Proc Natl
807 Acad Sci U S A, 2003. **100**(25): p. 15178-83.
808 11. Lan, X., et al., *Fate mapping of human glioblastoma reveals an invariant stem cell hierarchy.*
809 Nature, 2017. **549**(7671): p. 227-232.
810 12. Huang, W., et al., *The miR-26a/AP-2alpha/Nanog signaling axis mediates stem cell self-*
811 *renewal and temozolomide resistance in glioma.* Theranostics, 2019. **9**(19): p. 5497-5516.
812 13. Bao, S., et al., *Glioma stem cells promote radioresistance by preferential activation of the*
813 *DNA damage response.* Nature, 2006. **444**(7120): p. 756-60.
814 14. Lathia, J.D., et al., *Cancer stem cells in glioblastoma.* Genes Dev, 2015. **29**(12): p. 1203-17.
815 15. Pietras, A., et al., *Osteopontin-CD44 signaling in the glioma perivascular niche enhances*
816 *cancer stem cell phenotypes and promotes aggressive tumor growth.* Cell Stem Cell, 2014.
817 **14**(3): p. 357-69.
818 16. Wei, W., et al., *Single-Cell Phosphoproteomics Resolves Adaptive Signaling Dynamics and*
819 *Informs Targeted Combination Therapy in Glioblastoma.* Cancer Cell, 2016. **29**(4): p. 563-573.
820 17. Kalisky, T., P. Blainey, and S.R. Quake, *Genomic analysis at the single-cell level.* Annu Rev
821 Genet, 2011. **45**: p. 431-45.
822 18. Mund, A., et al., *Deep Visual Proteomics defines single-cell identity and heterogeneity.* Nat
823 Biotechnol, 2022. **40**(8): p. 1231-1240.
824 19. Hughes, R.E., et al., *Multiparametric High-Content Cell Painting Identifies Copper Ionophores*
825 *as Selective Modulators of Esophageal Cancer Phenotypes.*

20. O'Duibhir, E., N.O. Carragher, and S.M. Pollard, *Accelerating glioblastoma drug discovery: Convergence of patient-derived models, genome editing and phenotypic screening.* Mol Cell Neurosci, 2017. **80**: p. 198-207.
21. Subbiah, V., et al., *Dabrafenib plus trametinib in BRAFV600E-mutated rare cancers: the phase 2 ROAR trial.* Nat Med, 2023. **29**(5): p. 1103-1112.
22. Raswoli, M., et al., *Salvage chemotherapy after failure of targeted therapy in a child with BRAF V600E low-grade glioma.* Pediatr Blood Cancer, 2021. **68**(1): p. e28561.
23. Munjapara, V., et al., *BRAF V600E-Mutant Glioblastoma with Extracranial Metastases Responsive to Combined BRAF and MEK Targeted Inhibition: A Case Report.* Case Rep Oncol, 2022. **15**(3): p. 909-917.
24. Miller, K.E., et al., *Clinical response to dabrafenib plus trametinib in a pediatric ganglioglioma with BRAF p.T599dup mutation.* Cold Spring Harb Mol Case Stud, 2021. **7**(2).
25. Toll, S.A., et al., *Sustained response of three pediatric BRAF(V600E) mutated high-grade gliomas to combined BRAF and MEK inhibitor therapy.* Oncotarget, 2019. **10**(4): p. 551-557.
26. Newlands, E.S., et al., *Temozolomide: a review of its discovery, chemical properties, pre-clinical development and clinical trials.* Cancer Treat Rev, 1997. **23**(1): p. 35-61.
27. Moffat, J.G., et al., *Opportunities and challenges in phenotypic drug discovery: an industry perspective.* Nat Rev Drug Discov, 2017. **16**(8): p. 531-543.
28. Swinney, D.C. and J. Anthony, *How were new medicines discovered?* Nat Rev Drug Discov, 2011. **10**(7): p. 507-19.
29. Sadri, A., *Is Target-Based Drug Discovery Efficient? Discovery and "Off-Target" Mechanisms of All Drugs.* J Med Chem, 2023. **66**(18): p. 12651-12677.
30. Moffat, J.G., J. Rudolph, and D. Bailey, *Phenotypic screening in cancer drug discovery - past, present and future.* Nat Rev Drug Discov, 2014. **13**(8): p. 588-602.
31. Eder, J., R. Sedrani, and C. Wiesmann, *The discovery of first-in-class drugs: origins and evolution.* Nat Rev Drug Discov, 2014. **13**(8): p. 577-87.
32. Vincent, F., et al., *Developing predictive assays: the phenotypic screening "rule of 3".* Sci Transl Med, 2015. **7**(293): p. 293ps15.
33. Vincent, F., et al., *Publisher Correction: Phenotypic drug discovery: recent successes, lessons learned and new directions.* Nat Rev Drug Discov, 2022. **21**(7): p. 541.
34. Temps, C., et al., *A Conformation Selective Mode of Inhibiting SRC Improves Drug Efficacy and Tolerability.* Cancer Res, 2021. **81**(21): p. 5438-5450.
35. Bray, M.-A., et al., *Cell Painting, a high-content image-based assay for morphological profiling using multiplexed fluorescent dyes.* Nature Protocols, 2016. **11**(9): p. 1757-1774.
36. Rohban, M.H., et al., *Systematic morphological profiling of human gene and allele function via Cell Painting.* eLife, 2017. **6**: p. e24060-e24060.
37. Cimini, B.A., et al., *Optimizing the Cell Painting assay for image-based profiling.* bioRxiv, 2022: p. 2022.07.13.499171-2022.07.13.499171.
38. Way, G.P., et al., *Evolution and impact of high content imaging.* SLAS Discov, 2023. **28**(7): p. 292-305.
39. Caie, P.D., et al., *High-content phenotypic profiling of drug response signatures across distinct cancer cells.* Mol Cancer Ther, 2010. **9**(6): p. 1913-26.
40. Bray, M.A., et al., *A dataset of images and morphological profiles of 30 000 small-molecule treatments using the Cell Painting assay.* Gigascience, 2017. **6**(12): p. 1-5.
41. Perlman, Z.E., et al., *Multidimensional drug profiling by automated microscopy.* Science, 2004. **306**(5699): p. 1194-8.
42. Gustafsdottir, S.M., et al., *Multiplex Cytological Profiling Assay to Measure Diverse Cellular States.* PLoS ONE, 2013. **8**(12): p. 80999-80999.
43. Pollard, S.M., et al., *Glioma stem cell lines expanded in adherent culture have tumor-specific phenotypes and are suitable for chemical and genetic screens.* Cell Stem Cell, 2009. **4**(6): p. 568-80.
44. Codrici, E., et al., *Friends with Benefits: Chemokines, Glioblastoma-Associated Microglia/Macrophages, and Tumor Microenvironment.* Int J Mol Sci, 2022. **23**(5).
45. Fedele, M., L. Cerchia, and S. Battista, *Subtype Transdifferentiation in Human Cancer: The Power of Tissue Plasticity in Tumor Progression.* Cells, 2024. **13**(4).

881 46. Liu, H., et al., *Neutralizing IL-8 potentiates immune checkpoint blockade efficacy for glioma.*
882 Cancer Cell, 2023. **41**(4): p. 693-710 e8.
883 47. Bray, M.-A. and A.E. Carpenter, *Quality Control for High-Throughput Imaging Experiments*
884 *Using Machine Learning in Cellprofiler.* Methods in molecular biology (Clifton, N.J.), 2018.
885 **1683**: p. 89-112.
886 48. Hughes, R.E., et al., *High-Content Phenotypic Profiling in Esophageal Adenocarcinoma*
887 *Identifies Selectively Active Pharmacological Classes of Drugs for Repurposing and Chemical*
888 *Starting Points for Novel Drug Discovery.* SLAS Discovery, 2020. **25**(7): p. 770-782.
889 49. Warchal, S.J., et al., *High content phenotypic screening identifies serotonin receptor*
890 *modulators with selective activity upon breast cancer cell cycle and cytokine signaling*
891 *pathways.* Bioorg Med Chem, 2020. **28**(1): p. 115209.
892 50. Carpenter, A.E., et al., *CellProfiler: image analysis software for identifying and quantifying*
893 *cell phenotypes.* Genome Biol, 2006. **7**(10): p. R100.
894 51. Markossian, S., et al., *Assay Guidance Manual for Drug Discovery: Robust or Go Bust.* SLAS
895 Discov, 2021. **26**(10): p. 1241-1242.
896 52. Wells, C.I., et al., *The Kinase Chemogenomic Set (KCGS): An Open Science Resource for Kinase*
897 *Vulnerability Identification.* Int J Mol Sci, 2021. **22**(2).
898 53. Athanasiadis, P., et al., *Chemogenomic library design strategies for precision oncology,*
899 *applied to phenotypic profiling of glioblastoma patient cells.* iScience, 2023. **26**(7): p. 107209.
900 54. Omta, W.A., et al., *HC StratoMineR: A Web-Based Tool for the Rapid Analysis of High-Content*
901 *Datasets.* Assay Drug Dev Technol, 2016. **14**(8): p. 439-452.
902 55. Hastie, T., R. Tibshirani, and J.H. Friedman, *The elements of statistical learning : data mining,*
903 *inference, and prediction*. 2nd ed. Springer series in statistics,. 2009, New York, NY: Springer.
904 xxii, 745 p.
905 56. Asghar, U., et al., *The history and future of targeting cyclin-dependent kinases in cancer*
906 *therapy.* Nat Rev Drug Discov, 2015. **14**(2): p. 130-46.
907 57. Zhang, M., et al., *CDK inhibitors in cancer therapy, an overview of recent development.* Am J
908 Cancer Res, 2021. **11**(5): p. 1913-1935.
909 58. Olson, C.M., et al., *Pharmacological perturbation of CDK9 using selective CDK9 inhibition or*
910 *degradation.* Nat Chem Biol, 2018. **14**(2): p. 163-170.
911 59. Howard, D., et al., *Dinaciclib as an effective pan-cyclin dependent kinase inhibitor in platinum*
912 *resistant ovarian cancer.* Front Oncol, 2022. **12**: p. 1014280.
913 60. Howard, D., et al., *Dinaciclib, a Bimodal Agent Effective against Endometrial Cancer.* Cancers
914 (Basel), 2021. **13**(5).
915 61. Cidado, J., et al., *AZD4573 Is a Highly Selective CDK9 Inhibitor That Suppresses MCL-1 and*
916 *Induces Apoptosis in Hematologic Cancer Cells.* Clin Cancer Res, 2020. **26**(4): p. 922-934.
917 62. Chen, L., et al., *Functional characterization of TSPAN7 as a novel indicator for*
918 *immunotherapy in glioma.* Front Immunol, 2023. **14**: p. 1105489.
919 63. Arafeh, R., et al., *The present and future of the Cancer Dependency Map.* Nat Rev Cancer,
920 2025. **25**(1): p. 59-73.
921 64. Lee, S., et al., *High-throughput identification of repurposable neuroactive drugs with potent*
922 *anti-glioblastoma activity.* Nat Med, 2024. **30**(11): p. 3196-3208.
923 65. Ariey-Bonnet, J., et al., *Combination drug screen targeting glioblastoma core vulnerabilities*
924 *reveals pharmacological synergisms.* EBioMedicine, 2023. **95**: p. 104752.
925 66. Heinrich, B., et al., *Activity of cabazitaxel in temozolomide refractory glioblastoma: Final*
926 *results of a phase 2 study (C-GBM study; EudraCT 2013-001550-98 NCT 01866449).* Journal
927 of Clinical Oncology, 2017. **35**.
928 67. Goldlust, S.A., et al., *Phase 1 trial of TPI 287, a microtubule stabilizing agent, in combination*
929 *with bevacizumab in adults with recurrent glioblastoma.* Neurooncol Adv, 2024. **6**(1): p.
930 vdae009.
931 68. Silberman, S. and Z. Muzyczenko, *Updates on a Potentially Pivotal Trial Cns-201: A*
932 *Randomized, Controlled Trial of Berubicin Vs. Lomustine after First-Line Therapy for*
933 *Glioblastoma Multiforme (Gbm).* Neuro-Oncology, 2024. **26**.
934 69. Painuly, U. and S. Kumar, *Efficacy of bortezomib as first-line treatment for patients with*
935 *multiple myeloma.* Clin Med Insights Oncol, 2013. **7**: p. 53-73.

936 70. Gozdz, A., *Proteasome Inhibitors against Glioblastoma-Overview of Molecular Mechanisms*
937 *of Cytotoxicity, Progress in Clinical Trials, and Perspective for Use in Personalized Medicine.*
938 Curr Oncol, 2023. **30**(11): p. 9676-9688.
939 71. Iwamoto, F.M., et al., *A phase I/II trial of the histone deacetylase inhibitor romidepsin for*
940 *adults with recurrent malignant glioma: North American Brain Tumor Consortium Study 03-*
941 *03.* Neuro-Oncology, 2011. **13**(5): p. 509-516.
942 72. Lee, E.Q., et al., *Phase II study of panobinostat in combination with bevacizumab for*
943 *recurrent glioblastoma and anaplastic glioma.* Neuro-Oncology, 2015. **17**(6): p. 862-867.
944 73. Ghiaseddin, A., et al., *Phase II Study of Bevacizumab and Vorinostat for Patients with*
945 *Recurrent World Health Organization Grade 4 Malignant Glioma.* Oncologist, 2018. **23**(2): p.
946 157-e21.
947 74. Peters, K.B., et al., *Phase I/II trial of vorinostat, bevacizumab, and daily temozolomide for*
948 *recurrent malignant gliomas.* J Neurooncol, 2018. **137**(2): p. 349-356.
949 75. Bagley, S.J., et al., *Glioblastoma Clinical Trials: Current Landscape and Opportunities for*
950 *Improvement.* Clin Cancer Res, 2022. **28**(4): p. 594-602.
951 76. Karmur, B.S., et al., *Blood-Brain Barrier Disruption in Neuro-Oncology: Strategies, Failures,*
952 *and Challenges to Overcome.* Front Oncol, 2020. **10**: p. 563840.
953 77. Wu, S., et al., *All-stage targeted therapy for glioblastoma based on lipid membrane coated*
954 *cabazitaxel nanocrystals.* J Control Release, 2022. **345**: p. 685-695.
955 78. Chen, C., et al., *Hyaluronic Acid-Conjugated Nanoparticles for the Targeted Delivery of*
956 *Cabazitaxel to CD44-Overexpressing Glioblastoma Cells.* J Biomed Nanotechnol, 2021. **17**(4):
957 p. 595-605.
958 79. Madani, F., et al., *Polymeric nanoparticles for drug delivery in glioblastoma: State of the art*
959 *and future perspectives.* J Control Release, 2022. **349**: p. 649-661.
960 80. Mokarram, N., et al., *Device-assisted strategies for drug delivery across the blood-brain*
961 *barrier to treat glioblastoma.* Commun Mater, 2025. **6**(1): p. 5.
962 81. Ellert-Miklaszewska, A., et al., *Integrin Signaling in Glioma Pathogenesis: From Biology to*
963 *Therapy.* Int J Mol Sci, 2020. **21**(3).
964 82. Malric, L., et al., *Interest of integrins targeting in glioblastoma according to tumor*
965 *heterogeneity and cancer stem cell paradigm: an update.* Oncotarget, 2017. **8**(49): p. 86947-
966 86968.
967 83. Ortiz Rivera, J., et al., *Pyk2/FAK Signaling Is Upregulated in Recurrent Glioblastoma Tumors*
968 *in a C57BL/6/GL261 Glioma Implantation Model.* Int J Mol Sci, 2023. **24**(17).
969 84. Stettner, M.R., et al., *Lyn kinase activity is the predominant cellular SRC kinase activity in*
970 *glioblastoma tumor cells.* Cancer Res, 2005. **65**(13): p. 5535-43.
971 85. Du, J., et al., *Bead-based profiling of tyrosine kinase phosphorylation identifies SRC as a*
972 *potential target for glioblastoma therapy.* Nat Biotechnol, 2009. **27**(1): p. 77-83.
973 86. Lu, K.V., et al., *Fyn and SRC are effectors of oncogenic epidermal growth factor receptor*
974 *signaling in glioblastoma patients.* Cancer Res, 2009. **69**(17): p. 6889-98.
975 87. Lipinski, C.A., et al., *The tyrosine kinase pyk2 promotes migration and invasion of glioma*
976 *cells.* Neoplasia, 2005. **7**(5): p. 435-45.
977 88. Loftus, A.E.P., et al., *An ILK/STAT3 pathway controls glioblastoma stem cell plasticity.* Dev
978 Cell, 2024. **59**(24): p. 3197-3212 e7.
979 89. Tarin, M., et al., *FAK Inhibitor-Based Combinations with MEK or PKC Inhibitors Trigger*
980 *Synergistic Antitumor Effects in Uveal Melanoma.* Cancers 2023, Vol. 15, Page 2280, 2023.
981 **15**(8): p. 2280-2280.
982 90. McGivern, N., et al., *Activation of MAPK signalling results in resistance to saracatinib*
983 *(AZD0530) in ovarian cancer.* Oncotarget, 2017. **9**(4): p. 4722-4736.
984 91. Furqan, M., et al., *Drug Combinations Targeting FAK and MEK Overcomes Tumor*
985 *Heterogeneity in Glioblastoma.* Pharmaceutics, 2025. **17**(5).
986 92. Almazan, J., et al., *Combined inhibition of focal adhesion kinase and RAF/MEK elicits*
987 *synergistic inhibition of melanoma growth and reduces metastases.* Cell Rep Med, 2025.
988 **6**(2): p. 101943.

93. Fu, X., et al., *FOXA1 overexpression mediates endocrine resistance by altering the ER transcriptome and IL-8 expression in ER-positive breast cancer.* Proc Natl Acad Sci U S A, 2016. **113**(43): p. E6600-E6609.
94. Kim, J., et al., *FOXA1 inhibits prostate cancer neuroendocrine differentiation.* Oncogene, 2017. **36**(28): p. 4072-4080.
95. Langhans, J., et al., *The effects of PI3K-mediated signalling on glioblastoma cell behaviour.* Oncogenesis, 2017. **6**(11): p. 398.
96. Garros-Regulez, L., et al., *Targeting SOX2 as a Therapeutic Strategy in Glioblastoma.* Front Oncol, 2016. **6**: p. 222.
97. Zhang, Z. and Y. Zhang, *Transcriptional regulation of cancer stem cell: regulatory factors elucidation and cancer treatment strategies.* J Exp Clin Cancer Res, 2024. **43**(1): p. 99.
98. Singh, D.K., et al., *Oncogenes Activate an Autonomous Transcriptional Regulatory Circuit That Drives Glioblastoma.* Cell Rep, 2017. **18**(4): p. 961-976.
99. Bacon, C.W. and I. D'Orso, *CDK9: a signaling hub for transcriptional control.* Transcription, 2019. **10**(2): p. 57-75.
100. Olson, C.M., et al., *Pharmacological perturbation of CDK9 using selective CDK9 inhibition or degradation.* Nature chemical biology, 2018. **14**(2): p. 163-163.
101. Cidado, J., et al., *AZD4573 is a highly selective CDK9 inhibitor that suppresses Mcl-1 and induces apoptosis in hematologic cancer cells.* Clinical Cancer Research, 2020. **26**(4): p. 922-934.
102. Veeranki, O.L., et al., *Targeting cyclin-dependent kinase 9 by a novel inhibitor enhances radiosensitization and identifies Axl as a novel downstream target in esophageal adenocarcinoma.* Oncotarget, 2019. **10**(45): p. 4703-4718.
103. Orhan, E., et al., *CDK inhibition results in pharmacologic BRCAness increasing sensitivity to olaparib in BRCA1-WT and olaparib resistant in Triple Negative Breast Cancer.* Cancer Lett, 2024. **589**: p. 216820.
104. Cao, S., et al., *Inhibition of CDK9 induces apoptosis and potentiates the effect of cisplatin in hypopharyngeal carcinoma cells.* Biochem Biophys Res Commun, 2017. **482**(4): p. 536-541.
105. Ranjan, A., et al., *Targeting CDK9 for the Treatment of Glioblastoma.* Cancers (Basel), 2021. **13**(12).
106. Szklarczyk, D., et al., *The STRING database in 2023: protein-protein association networks and functional enrichment analyses for any sequenced genome of interest.* Nucleic Acids Res, 2023. **51**(D1): p. D638-D646.
107. Shannon, P., et al., *Cytoscape: a software environment for integrated models of biomolecular interaction networks.* Genome Res, 2003. **13**(11): p. 2498-504.
108. Zheng, S., et al., *SynergyFinder Plus: Toward Better Interpretation and Annotation of Drug Combination Screening Datasets.* Genomics Proteomics Bioinformatics, 2022. **20**(3): p. 587-596.